Pyridoxamine-phosphate oxidases and pyridoxamine-phosphate oxidase-related proteins catalyze the oxidation of 6-NAD(P)H to NAD(P)$^+$

Alexandre Y. Marbaix,[1,2] Georges Chehade,[1] Gaëtane Noël,[1] Pierre Morsomme,[3] Didier Vertommen,[4] Guido T. Bommer,[1,2] and Emile Van Schaftingen[1,2]

[1]Laboratory of Physiological Chemistry, de Duve Institute, UCLouvain, Brussels, B-1200, Belgium

[2]Walloon Excellence in Life Sciences and Biotechnology (WELBIO), UCLouvain, Brussels, B-1200, Belgium

[3]LIBST, UCLouvain, Louvain-la-Neuve, B-1348, Belgium

[4]PHOS Laboratory, de Duve Institute, UCLouvain, Brussels, B-1200, Belgium

[*]Corresponding author : emile.vanschaftingen@uclouvain.be

ABSTRACT

6-NADH and 6-NADPH are strong inhibitors of several dehydrogenases that may form spontaneously from NAD(P)H. They are known to be oxidized to $NAD(P)^+$ by mammalian renalase, an FAD-linked enzyme mainly present in heart and kidney, and by related bacterial enzymes. We partially purified an enzyme oxidizing 6-NADPH from rat liver, and, surprisingly, identified it as pyridoxamine-phosphate oxidase (PNPO). This was confirmed by the finding that recombinant mouse PNPO oxidized 6-NADH and 6-NADPH with catalytic efficiencies comparable to those observed with pyridoxine- and pyridoxamine-5'-phosphate. PNPOs from *Escherichia coli*, *Saccharomyces cerevisiae* and *Arabidopsis thaliana* also displayed 6-NAD(P)H oxidase activity, indicating that this 'side-activity' is conserved. Remarkably, 'pyridoxamine-phosphate oxidase-related proteins' (PNPO-RP) from *Nostoc punctiforme*, *A. thaliana* and the yeast *S. cerevisiae* (Ygr017w) were not detectably active on pyridox(am)ine-5'-P, but oxidized 6-NADH, 6-NADPH, and 2-NADH suggesting that this may be their main catalytic function. Their specificity profiles were therefore similar to that of renalase. Inactivation of renalase and of PNPO in mammalian cells and of Ygr017w in yeasts led to the accumulation of a reduced form of 6-NADH, tentatively identified as 4,5,6-$NADH_3$, which can also be produced *in vitro* by reduction of 6-NADH by glyceraldehyde-3-phosphate dehydrogenase or glucose-6-phosphate dehydrogenase. As 4,5,6-$NADH_3$ is not a substrate for renalase, PNPO or PNPO-RP, its accumulation presumably reflects the block in the oxidation of 6-NADH. These findings indicate that two different classes of enzymes using either FAD (renalase) or FMN (PNPOs and PNPO-RPs) as a cofactor play an as yet unsuspected role in removing damaged forms of NAD(P).

ABBREVIATIONS LIST

LC-MS liquid chromatography-mass spectrometry

PNPO : pyridoxamine-phosphate oxidase

PNPO-RP : pyridoxamine-phosphate oxidase related protein

PM5P : pyridoxamine-5'-phosphate

PN5P : pyridoxine-5'-phosphate

PL5P : pyridoxal-5'-phosphate

RNLS : renalase

KEYWORDS

metabolite-repair; 6-NADH; pyridine nucleotides, pyridoxamine-phosphate oxidase; enzyme-promiscuity; renalase.

INTRODUCTION

Mounting evidence indicates the importance of repair reactions in metabolism (1-4). Besides catalyzing their classical reactions, enzymes often display side activities on intracellular molecules that resemble their physiological substrate, thus forming non classical metabolites. Damaged or non canonical metabolites are also formed by numerous 'spontaneous' reactions (5) occurring at low, yet significant rates under in vivo conditions. These non-classical metabolites represent a burden to cells, as is best indicated by the discovery in recent years of several metabolite repair enzymes and the demonstration that several of them are indispensable. Deficiency in repair enzymes may indeed lead to diseases in humans or be lethal in mice (4). Thus, deficiency in L-2-hydroxyglutarate dehydrogenase, which serves to reconvert a metabolite formed by a side reaction of malate dehydrogenase or lactate dehydrogenase on alpha-ketoglutarate, leads to a leukoencephalopathy caused by the accumulation of L-2-hydroxyglutarate in brain (6-8). Deficiency in PGP, an enzyme that destroys the glycolytic side products and metabolic inhibitors 4-phosphoerythronate and L-2-phospholactate (9), is embryonic-lethal in mice (10). G6PC3, an endoplasmic reticulum protein formerly described as a 'ubiquitous glucose-6-phosphatase', was recently shown to be a metabolite repair enzyme that, in collaboration with the glucose-6-phosphate transporter G6PT, dephosphorylates the hexokinase inhibitor 1,5-anhydroglucitol-6-phosphate, and thereby prevents the development of a neutropenia (11).

Coenzymes and cofactors are vital for cellular metabolism, but due to their intrinsically high chemical reactivity, they are particularly prone to be converted to useless and potentially toxic forms. Thus, NAD and NADP may undergo different types of damage reactions. Hydration of their reduced form, either spontaneous or enzyme-catalyzed, leads to the formation of NAD(P)HX, where a hydroxyl group is bound to carbon 6 of the nicotinamide moiety (12,13). An ATP-dependent dehydratase reaction allows the (S)-form of NAD(P)HX to be reconverted to NAD(P)H, while the (R)-epimer is converted to the (S) form by an epimerase forming in bacteria a bifunctional protein with the dehydratase (14-16). Deficiency in either of these enzymes leads to major neurological problems and early death in humans (17-20).

Other forms of damaged nicotinamide nucleotides are species where the reduced atom on the nicotinamide ring is C6 or C2 (6-NADH and 2-NADH) rather than C4 as in classical NADH. These forms arise spontaneously during long-term storage of NADH solutions, resulting from the reduction of C6 or C2 of contaminating NAD^+ by NADH (21,22). 2-NADH is highly unstable, whereas 6-NADH is much more stable. Furthermore, this compound and 6-NADPH are strong inhibitors of several dehydrogenases, including lactate dehydrogenase and malate dehydrogenase (21,23). Renalase, a flavoprotein mainly expressed in kidneys and heart but absent or nearly absent from liver or brain was recently shown to catalyze the oxidation of 2- or 6-NAD(P)H (Fig. 1) (23-26).

Independently from the work on renalase, we initiated a few years ago investigations aimed at identifying an enzyme able to oxidize 6-NAD(P)H in rat liver. As described in the present work, this led us to the surprising observation that pyridoxamine-phosphate oxidase (PNPO) was a major 6-NAD(P)H oxidase in tissue extracts. Remarkably this capacity of oxidizing 6-NAD(P)H is highly conserved among PNPOs and seems to be the sole significant activity of some distant members of this family. We show also that inactivation of 6-NAD(P)H oxidizing enzymes in cells leads to the accumulation of a reduced from of 6-NADH, presumably 4,5,6-$NADH_3$. The purpose of this article is to report these findings.

Experimental

Reagents — Unless otherwise stated, chemicals were obtained from Sigma and Roche at the highest degree of purity.

Preparations of 2-NADH, 6-NADH and 6-NADPH — 2-NADH, 6-NADH and 6-NADPH were produced by reducing β-NAD^+ or β-$NADP^+$ with sodium borohydride (21). Briefly, 10 mg of $NAD(P)^+$ was dissolved in 0.5 ml of 0.05 M Tris buffer, pH 8.5 (Bio-Rad) and 50 µl of a 0.8 M $NaBH_4$ solution was added stepwise (volumes of 10 µl) to the stirred solution at room temperature. Then, 50 µl of 1 M glucose (Acros) was added to consume the excess of $NaBH_4$ and the mixture was loaded onto a 1 ml Q-Sepharose resin (GE Healthcare). Elution with a NaCl (Acros) gradient allowed the separation of 6-NAD(P)H from classical NAD(P)H. The fraction containing most of the 6-NAD(P)H was loaded on a semi preparative Pursuit Xrs 5 C18 reverse phase column (10.0 x 250 mm, 5 µM particle size) run at 4 ml/min with a mobile phase of 50 mM ammonium acetate (Merck), pH 7.0 and the NAD(P)H isomers were eluted with a gradient of 0 to 4% acetonitrile (HiperSolv). The elution of NAD(P)H and 6-NAD(P)H was followed both at 260 and 345 nm. 6-NAD(P)H was collected (~ 15 ml), loaded on a 1 ml Q-Sepharose column and eluted as described above to concentrate it and ensure that no trace of $NAD(P)^+$, which coelutes with 6-NAD(P)H in our HPLC method, remained in the solution. After lyophilization, the preparation of 6-NAD(P)H was resuspended in a suitable volume of 25 mM Tris, pH 8.0 and the concentration of the resulting solution was determined using ε_{345} = 6580 M^{-1} cm^{-1} (23). Purity of the solution was assessed both by enzymatic assay at 345 nm (see below) and by HPLC analysis using an analytic Polaris 5 C18-A reverse phase column (4.6 x 150 mm, 5 µM particle size) with the same gradient at 1 ml/min.

Due to the high lability of 2-NADH in the conditions of its synthesis (50 mM Tris pH 8.5), we were not able to purify it on HPLC. After reduction of NAD^+ as described above, we added sodium pyruvate (Merck) and rabbit lactate dehydrogenase (Roche) to oxidize 4-NADH whereupon the mixture was chromatographed on an anion exchange column and eluted with a NaCl gradient in order to separate NAD^+ from both 6-NADH and 2-NADH.

Purification and molecular identification of rat liver 6-NAD(P)H oxidase — Rat liver (~ 3.6 g) was homogenized in 4 volumes (w/v) of buffer A (25 mM Hepes, pH 7.1, 2 $\mu g.ml^{-1}$ of leupeptin and antipain; Peptide Institute, Osaka, Japan) containing 25 mM KCl (Acros) with a Potter glass teflon homogenizer. The homogenate was centrifuged at 16,000 x *g* for 15 min at 4°C. The resulting supernatant (18 ml) was diluted two-fold with buffer A and applied on a column containing ≈ 15 ml of DEAE-Sepharose equilibrated with buffer A. After washing with 50 ml buffer A, the retained proteins were eluted with a linear NaCl gradient (0-500 mM NaCl in 2 x 100 ml buffer A). The collected fractions (5 ml each) were tested for 6-NADPH oxidase activity by monitoring A_{345} to measure 6-NADPH consumption and the most active ones (15 ml) were pooled, diluted 2-fold with buffer A, and applied on a 9 ml Blue Trisacryl column equilibrated with the same buffer. After washing, the retained proteins were eluted with a linear NaCl gradient (0-2 M) in buffer A and 3.5 ml fractions were collected. The 6 most active fractions were pooled, concentrated to about 1.8 ml on a Vivaspin centrifugal concentrator. Solid NaCl was added to the concentrate to increase its NaCl concentration by 1

M and the preparation was applied on a column containing 0.5 ml Phenyl-Sepharose and equilibrated with buffer A containing 1 M NaCl. After washing, the retained proteins were eluted with a stepwise decreasing NaCl gradient (0.5, 0.2 and 0 M) followed by an increasing ethylene glycol gradient from 10 to 70 %). The activity was mostly eluted at 0.2 and 0 M NaCl. The most active fractions of the Blue Trisacryl and the Phenyl-Sepharose purification steps were analysed by nanoLC/MS/MS after trypsin digestion (27,28).

Cloning, expression, and purification of recombinant enzymes

The coding sequences of PNPO from *M. musculus* (NM_134021.2), *S. cerevisiae* (Pdx3; NM_001178383.1), *E. coli* (PdxH; NC_000913.3) and *A. thaliana* (PPOX1; NM_124376.4); of PNPO-RP from *A. thaliana* (PPOX2; NM_130223.3) and *S. cerevisiae* (Ygr017w; NM_001181146.1); and of *H. sapiens* renalase (RNLS; NM_001031709.3) were PCR-amplified using appropriate templates and primers (Table S1). The DNA sequence of PNPO-RP from *N. punctiforme* (WP_012411992.1) cloned in the pSpeedET vector was purchased from the DNASU plasmid repository (https://dnasu.org/DNASU/Home.do).

Mouse PNPO was expressed from the second ATG, to eliminate a mitochondrial propeptide predicted by TargetP (29). As the C-terminal residue in PNPOs and PNPO-RPs is a highly conserved proline, care was taken to avoid any C-terminal fusion. We therefore modified the ASKA clone allowing the expression of *E. coli* PNPO (PdxH), to remove a fused 4 amino acid C-terminal peptide (30). All genes were amplified using the *Pyrococcus furiosus* (Pfu; Promega) or *Phusion* (Thermofisher Scientific) proofreading DNA polymerases and inserted in the expression plasmids indicated in Table S2. The DNA sequence of each insert was checked by sequencing. All used vectors are designed for bacterial overexpression of N-terminally 6xHis-tagged protein upon induction with isopropyl-1-thio-β-D-galactopyranoside (IPTG) and all constructs were transformed in *E. coli* BL21 strains for subsequent expression (Table S2).

After expression, cells were pelleted by a 15 min centrifugation at 6000 x *g* and 4°C, suspended in a buffer containing 25 mM Hepes, 300 mM NaCl, 5 µg/ml antipain and leupeptin, 0.5 mM PMSF, 1 mg/ml lysozyme and 1 mM DTT. The pH of the buffer was 7.4 for mouse, yeast and E. coli PNPO, and PNPO-RP of *N. punctiforme*; and 7.1 for all the other proteins. Cell lysis was performed by freezing and thawing and DNA was digested as previously described (16). All the recombinant proteins were purified on a Ni-NTA chromatographic column (Thermofisher scientific). The cell lysate was diluted 3 fold in buffer A, containing 50 mM Hepes, pH 7.4, 300 mM NaCl, 10 mM imidazole; 2 µg/ml antipain, 2 µg/ml leupeptin and 5 µM FMN for each protein, except for RNLS, for which the buffer was 50 mM sodium phosphate, pH 8.0 and contained 5 µM FAD instead of FMN. The proteins were eluted with a linear imidazole gradient from 10 (buffer A) to 300 mM (buffer B). The fractions containing the protein of interest were pooled, concentrated by centrifugation in Vivaspin Turbo 15 filters (Sartorius) and desalted on PD-10 (GE Healthcare) columns.

Enzyme purity was estimated by SDS-PAGE and Coomassie Blue staining (Fig. S1). In all cases, the protein band of interest was the major one, and we did not make any correction in the calculation of the enzyme concentration by taking into account the presence of impurities. Protein concentration in the purified preparations was estimated by measuring

A_{280} and computing the concentration from the expected extinction coefficient on the basis of the amino acid composition (Protparam tool, at https://web.expasy.org/protparam/). Due to the uncertainty on the amount of FMN or FAD bound to the purified enzymes, we did not take into account the contribution of these coenzymes to A_{280}. This makes that we would overestimate the actual protein concentration of up to 1.36 and 1.48-fold, if there were in fact a stoichiometric amount of FMN or FAD bound to each subunit of the purified protein (based on calculations assuming ε280 values of 17,000 and 20,000 for FMN or FAD in solution). Taking this factor and the purity factor into account, we calculated that the actual values of V_{max} and catalytic efficiency were underestimated by ≈ 2-5 fold. This error does not affect the general interpretation of the data.

Spectrophotometric assays – The 6-NAD(P)H oxidase of PNPOs and PNPO-RPs (except the yeast enzyme) was assayed at 30°C in a buffer containing, unless otherwise indicated, 25 mM Hepes, pH 7.1, 20 mM KCl, 0.1 mg/ml BSA and 5 µM FMN. The activity of renalase was assayed under the same conditions except that 10 µM of FAD instead of 5 µM FMN was added in the reaction mixture. The enzymatic activity of *S. cerevisiae* PNPO-RP *(*Ygr017w was assayed at 30°C in a buffer comprising 50 mM sodium phosphate pH 7.0, 50 mM potassium acetate, 5 µM FMN and 0.1 mg/ml BSA. 6-NAD(P)H consumption was measured by monitoring A_{345} and the activity was calculated based on previously published values for the extinction coefficient of 6-NAD(P)H (ε_{345} = 6580 M^{-1} cm^{-1}) (23). Given the higher spontaneous rate of 2-NADH degradation at pH 7.1, the enzymatic assays of 2-NADH oxidase were performed both at pH 7.1 and at pH 8.5. 2-NADH consumption was measured by monitoring A_{395} and the activity was calculated based on an ε_{395} value of 5360 M^{-1} cm^{-1}) (23). Pyridoxamine-phosphate oxidase was assayed spectrophotometrically as described in Musayev et al (31).

Yeast strains, plasmids and media – S. cerevisiae strains were routinely grown on YPD medium (1% yeast extract, 2% peptone, 2% glucose) and/or minimal SD medium (0.67% yeast nitrogen base, 2% Complete Supplemented Mixture (CSM, MP Biomedicals), 2% glucose). The yeast strains used are listed in Table S3. The strains lacking the *PDX3* gene (Y13172) and the *YGR017W* gene (Y14647 and Y04647) were purchased from the Euroscarf systematic deletion library. The double-deletant *pdx3*Δ*/ygr017W*Δ was obtained both by crossing the single deletants Y13172 *pdx3*Δ *Mat* α and Y04647 *ygr017w*Δ *Mat a* or by PCR-mediated gene replacement in a single deletant strain, using as a selection marker the hygromycin B phosphotransferase gene. The hygromycin B gene fused to the TEF gene promoter and to the transcriptional terminator from the TEF gene was amplified from plasmid pAG34 (32). The primers used for the amplification of the resistance cassette, listed in Table S4, consisted of 53-56 nucleotides homologous to the genomic regions ≈ 45 nucleotides upstream or downstream of the targeted ORFs and a segment of 19-23 nucleotides homologous to the flanking regions of the hygromycin B resistance cassette. For each PCR reaction performed with *Phusion* polymerase, 50 ng of template and 50 pmoles of primers were used. Between 0.2 and 2 µg of PCR product was used to transform yeast cells according to the method described by Gietz and Schiestl (2007) (33). Transformed cells were then grown for 3 h at 30°C before being plated onto YPD plates containing 0.3 mg/ml

hygromycin B and 0.2 mg/ml kanamycin. After 48h, the transformants were grown in YPD containing 0.3 mg/ml hygromycin B and verified by analytical PCR on whole yeast colonies. The primers used to verify the correct disruption of the target gene are listed in Table S4.

Metabolite analysis of yeast cells – Yeast cells were grown in minimal medium until OD_{600} reached ≈ 1 to 1.5, which corresponded to the exponential growth phase. 5 ml of each culture were then rapidly sampled by fast vacuum filtration on polyethersulfone membrane (25 mm, 0.45 µm pore size, PALL corporation, Michigan, USA) and the scraped cell pellets were directly dipped in liquid nitrogen. The pellets were subsequently resuspended in 1.5 ml of the extraction solution (composed of 10 % water and 90% (v/v) of a mixture of 90% (v/v) methanol — Biosolve BV, The Netherlands — and 10% of $CHCl_3$ — Biosolve BV, The Netherlands) and the cells were lysed by 30 min of strong agitation in the presence of glass beads (Sigma-Aldrich) at 4°C. After 2 min of centrifugation at 16,000 x *g*, 350 µl of the upper phase was collected and vacuum-dried. The pellets were resuspended in 25 µl water, centrifuged as above and 5 µl of the supernatant was analysed by LC-MS as described below.

Gene inactivation in mammalian cells with CRISPR/Cas9 – According to the BioGPS website (www.biogps.org), the mRNA expression level of renalase in Human Colon Cancer HCT116 cells is about 100-fold lower than that of *PNPO* and our qPCR experiments showed that the abundance of renalase mRNA in these cells is below the detection level. On the other hand, comparable levels of renalase and PNPO mRNA were detected in bone osteosarcoma U2OS cells. The different primer pairs (3 for PNPO, 4 for RNLS) used to inactivate the PNPO (in U2OS and HTC116 cells) or the renalase gene (only in U2OS cells) are shown in Table S5. The PNPO gene was targeted in two different regions. Pairs 1 and 2 targeted exon 3 containing the conserved 'SRK' motif that is important for FMN-binding (31) and resulted in clones HCT116 B6 and C9 and U2OS ΔPNPO1. Pair 3 targeted the junction between exon 5 and exon 6 and resulted in clone U2OS ΔPNPO2. The RNLS gene was also targeted in two different regions. Pairs 1 and 2 targeted the second exon of the gene, which contains the conserved 'AQY' motif that is important for the FAD-binding in the catalytic pocket (34) and resulted in clone U2OS ΔRNLS1. Pairs 3 and 4 targeted the fifth exon of the gene, containing Arg193, which is presumably important for the catalytic activity (34) and resulted in clone U2OS ΔRNLS2. Annealed primers were ligated into the vector pSpCas9(BB)-2A-Puro (pX459) V2.0 and pSpCas9(BB)-2A-GFP (pX458) (a gift from F. Zhang, Massachusetts Institute of Technology ; Addgene plasmid #48139 and #48138, respectively) digested with BbsI and constructs were validated by sequencing (Beckman Coulter Genomics). HCT116 cells, a gift from E. Fearon (University of Michigan, Ann Arbor), and U2OS cells were cultivated in DMEM (Dulbecco's modified Eagle's medium) containing 10% FBS, 2 mM L-glutamine, penicillin/streptomycin (Life Technologies) and 4 mg/l pyridoxal (Sigma) to allow pyridoxal-phosphate formation by pyridoxal kinase in cells lacking PNPO. CRISPR pX459 constructs were transfected and selected with puromycin as described in Collard et al., 2016 (9). Genomic DNA of puromycin-resistant clones was used to PCR-amplify the regions encompassing the targeted sites and sequencing of the PCR products was used to identify any genetic modification in each clone.

The HCT116 clones used in this study had the following mutations:

ΔPNPO B6: change in the reading frame due to deletion of a 'G' between 'T296' and 'A298' of the DNA sequence, leading to a premature stop codon after 145 amino acids.
ΔPNPO C9: change in the reading frame due to insertion of a 'T' between 'T296' and 'G297' of the DNA sequence, leading to a premature stop codon after 111 amino acids.

The U2OS clones used in this study had the following mutations:
ΔPNPO1: change in the reading frame due to insertion of a 'T' between 'T296' and 'G297' of the DNA sequence, leading to a premature stop codon after 111 amino acids.
ΔPNPO2: change in the reading frame due to deletion of 'G543' and 'G544' of the DNA sequence, leading to a premature stop codon after 187 amino acids.
ΔRNLS1: deletion of 73 nucleotides between 'A151' and 'G224', leading to a premature stop codon after 56 amino acids.
ΔRNLS2: deletion of 49 nucleotides between 'A528' and 'G578', leading to a premature stop codon after 216 amino acids.

To generate double knockout clones (ΔPNPO/ΔRNLS) in the U2OS cell lines, ΔPNPO1 cells were transfected with RNLS CRISPR pX458 constructs and GFP positive cells were cloned after flow activated cell sorting with a BD FACSARIA III in 96-well plate (nozzle: 100µm, drop frequency: 30kHz, sheath pressure: 20 psi, precision mode : single cell) and expansion at 37°C during several days. Genomic DNA of the growing cells was then PCR-amplified and sequenced as described above. This resulted in two U2OS ΔPNPO/ΔRNLS clones that had the following mutations in the RNLS gene:
ΔPNPO/ΔRNLS1: Change of the reading frame due to deletion of A151, leading to a premature stop codon after 80 amino acids.
ΔPNPO/ΔRNLS2: Change of the reading frame due to insertion of a 'A' after 'A151', leading to a premature stop codon after 56 amino acids.
To complement the deficient cell lines, we generated lentiviral vectors for expression of either human PNPO or human RNLS or *A. thaliana* PPOX2. The coding sequence of each gene was PCR-amplified from minipreps using *Pfu* polymerase with primers listed in Table S6 and was cloned in a lentiviral vector derived from pLVX-puro (Clontech) vector between the BamHI and BsrGI restriction sites. HEK293T cells were transfected with 2 µg of these plasmids together with 2 µg of psPAX2 plasmid and 1 µg of pMD2 plasmid (Addgene plasmids # 12260 and #12259, kind gift from Didier Trono), which are two vectors allowing the production of the envelope and the viral capsule, using JetPEI DNA transfection agent (Polyplus transfection). After 48h at 37°C, the medium of HEK293T cells was collected, filtered on 0.45 µm filters (Filtropur) and mixed with 8 µg/ml polybrene (Sigma) before being added on U2OS deficient cells. After 18h at 37°C, the culture medium was replaced by the same medium containing 2 mg/ml of puromycin to select the infected cells. Complemented cells were then normally cultivated and complementation was assessed by qPCR experiment (not shown).

Metabolite analysis of U2OS cells – U2OS cells were plated at 600,000 cells per dish in 6 cm dishes and incubated in DMEM containing 4 mg/l pyridoxal for 48 h before harvesting. To quench metabolic activity, medium was removed, cells were quickly rinsed with ice-cold water and plates were plunged in liquid nitrogen (35). One ml of a 90% methanol/chloroform (9/1) mixture kept on dry ice was added on the still frozen plates. Cells were scraped and the

extracts were collected and centrifuged for 10 min at 16,000 x *g*. After vacuum-drying of the upper aqueous phase, the pellet was suspended in 30 µl of water, centrifuged for 2 min at 16,000 x *g* and 5 µl of the supernatant was analysed by LC-MS. LC-MS analysis was performed using the method as detailed in Veiga da Cunha et al. 2019 (11). Extracted ion chromatograms of the [M-H+]- forms were integrated using MassHunter software (Agilent, Santa Clara, CA, USA), and areas were normalized to total ion current. LC-MS results were obtained in at least three independent experiments where each experimental value is the mean of three technical replicas.

Quantitative PCR analysis of mice tissues – RNA from mouse tissues was extracted using TRIzol® reagent (Life Technologies) and reverse transcription was performed using RevertAID reverse transcriptase (Thermo Scientific) according to the manufacturer protocol using 2 µg RNA in a total volume of 20 µl. Five µl of 20-fold diluted cDNAs were used for quantitative PCR in a MyiQ^{TM} thermal cycler using SYBR Green as a fluorescent dye (Bio-Rad) and hotGoldStar *Taq* polymerase (Eurogentec, Seraing, Belgium). PCR programs were 95°C for 3 min, 40 cycles at 95°C for 10 s and 60°C for 1 min, with acquisition of fluorescence information, followed by a melting curve. Experiments shown represent means and standard deviations for three biological replicates. Primers used are listed in Table S7.

RESULTS

Identification of PNPO as a major 6-NAD(P)H metabolizing enzyme in liver extracts

A spectrophotometric assay at 345 nm indicated that 10 μM 6-NADPH was consumed at a rate of ≈ 40 nmol/min/g tissue in a rat liver high-speed supernatant, suggesting the existence of a 6-NADPH oxidase. Chromatography of a rat liver extract on DEAE-Sepharose showed that the putative 6-NADPH oxidase activity was eluted as a single peak with the salt gradient (Fig. 2). Further purification on Blue Trisacryl indicated that the enzyme was adsorbed on this type of column and eluted with high salt concentrations (not shown). A final step on Phenyl Sepharose yielded an enzyme whose specific activity was about 3-fold higher than in the eluate of the Blue Trisacryl column and about 100-fold higher than in the liver extract. The most active fractions of the Blue Trisacryl column and of the Phenyl Sepharose column were analyzed separately after trypsin digestion by tandem mass spectrometry. 123 proteins were identified by the detection of at least two different peptides in the Blue Trisacryl fraction and 82 in the Phenyl Sepharose fraction. Among the 123 proteins identified in the Blue Trisacryl column, 12 were oxidoreductases. We quantified their relative abundance in the Blue Trisacryl and Phenyl Sepharose fractions by dividing the numbers of 'peptide spectral matches' by the mean spectral match for each of the two fractions (Table S8). Comparison of the figures indicated that two oxidoreductases were enriched at least two-fold by the last chromatographic step: pyridoxamine-phosphate oxidase (PNPO) and 3-hydroxyanthranilate-3,4-dioxygenase (Table S8).

As PNPO is strongly inhibited by its classical product, pyridoxal-phosphate (31,36), we checked if the latter compound inhibited the oxidation of 6-NADPH by the enzyme purified from liver and found indeed that 1 μM pyridoxal-phosphate inhibited the enzymatic activity by more than 90 % (not shown). We also retrospectively measured the oxidase activity on pyridoxamine-phosphate in the fractions of the DEAE-Sepharose column and found near-perfect co-elution of this activity with the 6-NADPH consuming activity (Fig. 2).

Characterization of the activity of mouse pyridoxamine-phosphate oxidase on 6-NAD(P)H

Purified recombinant mouse PNPO catalyzed the oxidation of 6-NADPH and 6-NADH, and at lower rates, 2-NADH (Table 1) while it had no activity on NADH and NADPH (not shown). Kinetic analysis indicated that 6-NADPH was about 10-fold better as a substrate than 6-NADH (in terms of catalytic efficiency — k_{cat}/K_M in Table 1). We compared this activity to that measured spectrophotometrically on pyridoxamine-5'-phosphate (PM5P) and pyridoxine-5'-phosphate (PN5P), in the presence of 200 mM Tris, pH 8.5, to trap the produced pyridoxal-5'-phosphate (PL5P) as a Schiff's base (31). The results indicated that the catalytic efficiency for 6-NADPH was of the same order of magnitude as observed with PN5P and PM5P (Table 1). To ensure that PNPO converted 6-NAD(P)H to $NAD(P)^+$, we assayed the formed $NAD(P)^+$ by reducing it to NAD(P)H in the presence of glucose-6-phosphate and glucose-6-phosphate dehydrogenase (G6PDH) from *Leuconostoc mesenteroides* (which acts on both NAD^+ and $NADP^+$ (37). These assays showed that $NAD(P)^+$ formation exactly matched the disappearance of 6-NAD(P)H (not shown). We also checked if, as for PM5P and PN5P oxidation, H_2O_2 was the second product of the reaction. Reaction mixtures where a defined amount of 6-NADH had been consumed, as determined spectrophotometrically by the decrease in A345 (not shown), were then tested spectrophotometrically for the presence of H_2O_2, with a peroxidase assay based on the conversion of o-dianisidine to its oxidized form at

A460 (not shown) (27). This type of assay led us to the conclusion that 6-NAD(P)H disappearance was stoichiometric with the formation of H_2O_2.

Some PNPO-related proteins (PNPO-RPs) are excellent 6-NAD(P)H oxidases but lack PNPO activity

To better appreciate the potential importance of 6-NAD(P)H oxidation by PNPO, we tested PNPOs from other species. We included in our analysis three enzymes (Pdx3 from *Saccharomyces cerevisiae*, PPOX1 from *Arabidopsis thaliana* and PdxH from *Escherichia coli*), which have all been characterized previously (38-40). As shown in Table 1, all enzymes were active on 6-NADPH and 6-NADH, though the best substrate for all of them was PN5P. The catalytic efficiency for 6-NADPH was comparable to that observed with PM5P, and about 2-times higher than for 6-NADH. No activity was observed with 2-NADH with the two enzymes tested (Table 1).

We also tested three enzymes that belong to the PNPO family, but are only distantly related to *bona fide* PNPO, and which we call therefore PNPO-related proteins or PNPO-RP. A model enzyme in this category is AtPPOX2 from *A. thaliana* (encoded by the At2g46580 gene), which was previously studied and displays at best only a very low oxidase activity on PM5P or PN5P (< 1 % of activity of *A. thaliana* PNPO) (41). We also included in our studies PNPO-RP of the cyanobacterium *Nostoc punctiforme*, whose 3D structure is available (2i51 in pdb), and of *Saccharomyces cerevisiae* (Ygr017w), which share 38 % and 32 % sequence identity with AtPPOX2, respectively. All three enzymes were remarkably active on 6-NADH and 6-NADPH, with catalytic efficiencies that were at least as high as those observed with human renalase (Table 2) and about 2 orders of magnitude higher than observed with the 'true' pyridox(am)ine-phosphate oxidase (with the exception of mouse PNPO). As for mouse PNPO, we confirmed that the products of the reaction were $NAD(P)^+$ and H_2O_2 and that they were produced stoichiometrically. We also noted that these enzymes were very active on 2-NADH, even more so than renalase (Table 2). No activity was observed with 4-NADH, 4-NADPH, PM5P and PN5P (tested at up to 25 μM). Renalase was also lacking activity on these substrates.

We also determined the sensitivity of the 6-NAD(P)H oxidase activity of all these enzymes to pyridoxal-5'-phosphate (PL5P). We anticipated that this compound would strongly inhibit this activity in the case of the 'true' PNPOs, but not in the case of PNPO-RPs or renalase. We indeed observed that *M. musculus* and *S. cerevisiae* PNPOs were both strongly inhibited by PL5P. In the case of mouse and yeast PNPO, 50 % inhibition was reached at 0.5 and 20 μM, respectively, when the enzyme was tested in the presence of 25 μM 6-NADH. None of the PNPO-RPs, nor renalase was inhibited by PL5P (at a concentration of 10 μM).

Differences in key residues between PNPOs and PNPO-RPs may explain differences in specificity.

Fig. 3 shows a sequence alignment of the investigated enzymes. PNPOs share a series of highly conserved residues (highlighted in cyan) with PNPO-RPs. The two groups of enzymes differ by residues that are either conserved in the PNPOs (grey) or in PNPO-RPs (yellow). Strikingly, His199 and Arg197, which are known to interact directly with PN5P in PNPO (42) are not conserved in the PNPO-RPs. The structure of PNPO-RP from *Nostoc punctiforme* has been solved and deposited in the PDB databank. Like PNPOs (31), PNPO-RP is dimeric and binds two FMNs per dimer. Fig. 4 shows the structure around one of the two FMNs. Most of the residues that line the putative catalytic site at the upper face of FMN are conserved in both

PNPOs and PNPO-RPs (cyan) or only in PNPO-RPs (yellow). One of these PNPO-RP-specific residues is Arg45, which replaces a highly conserved lysine (Lys62 in *E. coli* PNPO) interacting with the phosphate group of PN5P in PNPO. Thinking that this residue might bind one of the phosphate groups of 6-NADH, we mutagenized it to alanine and found that this mutation markedly increased the K_M for 6-NADH (from < 5 μM to 115 μM) (Fig. S2). No significant change in the activity was observed when reduced N-methylnicotinamide was used as a substrate, confirming that Arg45 interacts with negatively charged groups of 6-NADH.

The alignment shows also that yeast PNPO-RP is characterized by a series of peptide insertions. These insertions, which were also found in many other PNPO-RPs from fungi (not shown), are not conserved in their length or their sequence and their relevance remains to be determined.

6-NAD(P)H can be further reduced by some dehydrogenases

Carbon 4 of the nicotinamide ring in 6-NAD(P)H is in the oxidized state. Therefore, we considered the possibility that it might be reduced by a side activity of some classical dehydrogenases. To test this, we incubated 6-NADH or 6-NADPH with several dehydrogenases together with their reduced substrate and followed A_{345}. We noted that in the presence of glyceraldehyde-3-phosphate dehydrogenase (from pig heart or *S. cerevisiae*), glyceraldehyde-3-phosphate and arsenate to stimulate the reaction, A_{345} decreased progressively while A_{290} increased (Fig. 5A). We determined that with 25 μM 6-NADH the specific activity of GAPDH was about 4.8 nanomoles/min/mg of protein, which corresponds roughly to 0.3 % of its specific activity under the same conditions but in presence of 25 μM NAD^+ instead of 6-NADH.

We noted similar changes in A_{345} and A_{290} when 6-NADPH was incubated with glucose-6-phosphate dehydrogenase (from yeast or *L. mesenteroides*) and glucose-6-phosphate or when 6-NADH was incubated with *L. mesenteroides* glucose-6-phosphate dehydrogenase and glucose-6-phosphate (Fig. 5B). LC-MS analysis revealed the appearance of a 'superreduced' form of 6-NADH, which coeluted with 6-NADH and had a m/z of 666.133, indicating the presence of two additional hydrogens (Fig. 5C). As these dehydrogenases normally transfer a hydride to C4 of the nicotinamide ring of $NAD(P)^+$, it is highly likely that they do the same when reducing 6-NADH. The most likely structure of the superreduced form is therefore 4,5,6-$NADH_3$. This conclusion is supported by the similarity of its absorbance spectrum with that of NADHX (12), a compound differing from 4,5,6-$NADH_3$ by the presence of oxygen on carbon 5, but with the same double bond distribution (Fig. 5D).

Other tested enzymes (lactate dehydrogenase with 1 mM lactate; isocitrate dehydrogenase with 1 mM isocitrate, glycerol-3-phosphate dehydrogenase with 0.25 mM glycerol-3-phosphate, alcohol dehydrogenase with 1 mM ethanol; glutamate dehydrogenase with 1 mM glutamate; L-malate dehydrogenase with 1 mM L-malate) did not allow the reduction of 6-NADH or 6-NADPH.

Of note, spectrophotometric assays indicated that neither 4,5,6-$NADH_3$, nor 4,5,6-$NADPH_3$ (tested at 10 μM) were substrates for human renalase, yeast or *A. thaliana* PNPO-RP, or mouse PNPO. Unlike 6-NADH (21,23,43), 4,5,6-$NADH_3$ was not a strong inhibitor of L-lactate dehydrogenase, L-malate dehydrogenase or alcohol dehydrogenase.

Respective abundance of RNLS and PNPO in mouse tissues by RT-qPCR

RT qPCR experiments indicated that the mRNA encoding renalase was most abundant in mouse heart, skeletal muscle, testis, kidney and lung (Fig. 6). In contrast, PNPO mRNA was

particularly abundant in liver followed by kidney, heart, spleen, skeletal muscle and brain. Liver was particularly remarkable in having very little renalase mRNA and the highest level of PNPO mRNA. High PNPO/renalase ratios were also observed in brain, spleen and kidneys, while on the contrary, a very high renalase/PNPO ratio was found in testis.

Effect of 6-NADH oxidase deficiency in mammalian cells and yeasts

To evaluate the respective role of renalase and PNPO in the utilization of 6-NADH in mammalian cells, we used the CRISPR-Cas9 technology to inactivate the PNPO gene (ΔPNPO), the RNLS gene (ΔRNLS) or both (ΔPNPO/ΔRNLS) in U2OS cells, which normally express the mRNAs of both proteins (not shown). We ensured by PCR amplification and sequencing that the two alleles of PNPO and the three alleles of RNLS were inactivated in single knockout (ΔPNPO and ΔRNLS) or double knockout clones (ΔPNPO/ΔRNLS) of U2OS cells.

The same number of cells of each clone and of wild type (WT) cells were cultivated for 48h in the presence of 25 μM pyridoxal, to avoid PL5P shortage in PNPO-deficient cells. After quenching, intracellular metabolites were analyzed by LC-MS. As expected, ΔPNPO cells showed a clear accumulation of PN5P (Fig. 7A). 6-NADH was detected as a peak with m/z 664.1175 that preceded the main peak of NADH by about 1 min. In U2OS cells, the 6-NADH peak was detected in extracts of all cells and was slightly (about 2-fold) but not significantly increased in cells that were deficient in renalase and/or PNPO (Fig. 7B). Its signal amounted to about 1 % of the main NADH peak. Similarly, a small peak of 6-NADPH, just before the NADPH peak, was detected in all cell extracts reaching about the same level (not shown).

We also noted a striking accumulation of 4,5,6-$NADH_3$ in cells deficient in renalase, whether simple or double mutants whereas this metabolite was almost absent in control cells or PNPO-deficient cells compared to ΔRNLS cells (Fig. 7C). No accumulation of 4,5,6-$NADPH_3$ was noted under any condition.

Complementation of double mutants (ΔPNPO/ΔRNLS) with human renalase, human PNPO, or both reduced the level of 6-NADH (significantly in clone 1 but not in clone 2) while complementation with *A. thaliana* PNPO-RP led to the disappearance of the 6-NADH peak. All complementations led also to a marked, significant decrease in the 4,5,6-$NADH_3$ peak in both clones (Fig. 7D-F).

Analysis of metabolites of the main metabolic pathways (glycolysis, the pentose-phosphate pathway, citric acid cycle) did not allow us to detect significant changes that could be attributed to deficiency in renalase or in PNPO (data not shown).

We also investigated the role of PNPO in the metabolism of 6-NAD(P)H in HCT116, which do not show detectable expression of the renalase mRNA and about 3-time higher level of PNPO mRNA. Since renalase is not expressed, we only inactivated the PNPO gene in this cell line. PNPO inactivation caused a significant accumulation not only of PN5P, but also of 4,5,6-$NADH_3$. This indicates, that in the case of these cells, PNPO is involved in the destruction of 6-NADH (Fig. S3).

We similarly evaluated the effect of PNPO-RP (Ygr017w) and PNPO (Pdx3) deficiency in yeasts and found that the defect in PNPO-RP caused a significant increase in 4,5,6-$NADH_3$ (Fig. 8). The defect in PNPO had no such effect, though it caused a marked increase in PN5P. Neither PNPO-RP, nor PNPO deficiency caused a significant change in 6-NADH. Again, analysis of metabolites of the main metabolic pathways did not disclose significant changes that could be attributed to deficiency in PNPO or PNPO-RP (note that pyridoxal is added to the cultures in all experiments where PNPO mutants are tested).

DISCUSSION

A new family of 6-NADH oxidases

Previous work has revealed the importance of repair mechanisms for damaged forms of metabolites and cofactors (1-4). The spontaneous *in vitro* formation of 6-NADH and 2-NADH in solutions of NADH by transfer of reducing equivalents from 4-NADH to NAD^+, suggests that this type of reaction may also occur in living cells. As 6-NADH and 6-NADPH are strong inhibitors of several dehydrogenases (21,23), it is logical to hypothesize that a repair enzyme may exist to eliminate these molecules. Studies on the flavoprotein renalase have shown that this protein, both in mammals and in Pseudomonads, is a very efficient oxidase for 6- and 2-NAD(P)H *in vitro* (23,24,26), but it was unknown whether renalase is required to prevent accumulation of 6-NAD(P)H or 2-NAD(P)H in intact cells or organisms.

We now report the existence of a second type of 6-NAD(P)H oxidases, which uses FMN instead of FAD as a cofactor. These enzymes are related to PNPOs, but have little or no action on PN5P or PM5P and they show catalytic efficiencies on 6-NADPH and 6-NADH of the same order of magnitude as human renalase. They differ from *bona fide* PNPOs by a series of residues, some of which have been shown to directly interact with pyridoxine-phosphate by crystallographic analysis of *E. coli* PNPO (42). As these enzymes generally act well on 6-NADH or 6-NADPH and as we have evidence for the utilization of 6-NADH in intact cells (see below), we propose to name them 6-NAD(P)H oxidase (FMN), while renalases would be called 6-NAD(P)H oxidase (FAD).

Remarkably, the four *bona fide* PNPOs that we have tested all show some 6-NADH and 6-NADPH oxidase activity, though with catalytic efficiencies that are lower than those observed with renalase or PNPO-RPs. This suggests that the oxidation of 6-NAD(P)H may be the primitive function of the ancestral protein that gave rise to present day PNPOs and 6-NAD(P)H oxidases (FMN).

Strikingly, renalase and PNPO-RPs act *in vitro* both on 6- and 2-NADH but not on 4-NADH. The structure of renalase with 4-NADH shows that the catalytic site is quite open and that the nicotinamide of NADH binds in such a way that its C2 juxtaposes to N5 of dimethylisoalloxazine moiety of FAD, which serves as hydride acceptor (24). Oxidation of 6-NADH can be easily understood by considering that rotation of the nicotinamide moiety along the bond between N1 of the nicotinamide and C1 of the ribose brings C6 in the appropriate position for hydride transfer (24). This is not true for 4-NADH which remains at a distance from N5 of dimethylisoalloxazine. It is likely that the same type of structural consideration also applies to PNPO-RPs, which have also a wide open catalytic site (see Fig. 4).

The action of PNPO on 6-NAD(P)H is inhibited *in vitro* by low concentrations of PL5P and it is therefore likely that PL5P, as well as the classical substrates PN5P and PM5P, may hamper the action of PNPOs on 6-NAD(P)H. This inhibition is not observed with the PNPO-RPs, which are therefore likely to be unaffected by vitamin B6 derivatives in their putative repair role for pyridine nucleotides.

Evidence for the repair role of 6-NADH oxidases in intact cells

The data that we have obtained on knockout cells support the idea that PNPO-RP (Ygr017w) in yeasts, as well as renalase and PNPO in mammalian cells destroy 6-NADH. This conclusion is based on measurements of both 6-NADH and of its reduced form 4,5,6-$NADH_3$. We start by discussing the latter measurements because they give a clearer picture.

We observed both in yeasts deficient in Ygr017w and in renalase-deficient human cells, a clear increase in the concentration of a compound that has the same molecular mass and elution profile as 4,5,6-$NADH_3$. As 4,5,6-$NADH_3$ is not a substrate for renalase, PNPO-RPs or PNPOs, its accumulation must reflect the accumulation of 6-NADH. The activity of glyceraldehyde-3-phosphate dehydrogenase with 6-NADH was approximately 0.3 % of its physiological activity using NAD^+. Given the high abundance of GAPDH in cells, increases in cytoplasmic 6-NADH might therefore efficiently be converted into 4,5,6-$NADH_3$, which, in contrast to 6-NADH, does not inhibit cellular dehydrogenases.

Remarkably, wild type U2OS cells and wild type yeasts have no detectable 4,5,6-$NADH_3$, and its level increases by more than tenfold if renalase or Ygr017w is knocked out. Complementation of the double knock out U2OS cells with human PNPO, human renalase or *A. thaliana* PNPO-RP all markedly reduce the 4,5,6-$NADH_3$ level, consistent with their ability to metabolize 6-NADH. It should be noted that a strong promoter has been used for this complementation. This may explain that PNPO has a marked negative effect on the 4,5,6-$NADH_3$ level in the complementation experiment, while the PNPO-deficient (single knockout) U2OS cells do not show any significant increase in 4,5,6-$NADH_3$ compared to the wild type cells. These observations nonetheless indicate that PNPO may participate in 6-NADH elimination in intact cells.

Observations made with HCT116 cells, which, for an unknown reason, do not express renalase, but show a higher level of PNPO mRNA than U2OS cells, are consistent with this interpretation. Unlike U2OS cells, wild type HCT116 cells do have a detectable amount of 4,5,6-$NADH_3$, supporting the important role played by renalase in eliminating 6-NADH. The increase in the level of this damaged nucleotide upon inactivation of PNPO further indicates that this enzyme, if sufficiently expressed, may participate in 6-NADH metabolism. As all experiments have been performed in the presence of 25 µM pyridoxal (to avoid the side effects of PL5P deficiency due to inactivation of the PNPO gene), our data presumably lead to underestimate the participation of PNPO. This might explain, for instance, the fact that the double mutant U2OS cells do not have more 4,5,6-$NADH_3$ than the single renalase mutant.

The interpretation of 6-NADH measurements is more complicated. The changes in 6-NADH levels generally show a similar trend as 4,5,6-$NADH_3$, but the relative changes in the concentration of 6-NADH are much smaller than those of 4,5,6-$NADH_3$, due to the presence of a rather variable background level of 6-NADH. We interpret this background level as resulting, at least partly, from the artefactual formation of 6-NADH during the concentration step taking place during the preparation of the samples for LC-MS analysis. We noted indeed that when mixtures of NAD(P)H and $NAD(P)^+$, at low concentrations (0.5 µM and 5 µM, respectively), were submitted to this concentration procedure, significant amounts of 6-NADH were formed ($\approx$ 2 % of the initial NADH) presumably through a spontaneous hydride transfer occurring between NADH and NAD^+ (22). Another explanation related to cell compartmentalization may also be considered. If, for instance, neither renalase nor PNPO are significantly active in the mitochondria (less than 5 % of PNPO activity is present in the mitochondria in liver (44); renalase has never been reported to be present in mitochondria), the 6-NADH that forms through spontaneous reactions in these organelles will accumulate. If furthermore mitochondria do not contain any enzyme capable of reducing 6-NADH to 4,5,6-$NADH_3$, this background of mitochondrial 6-NADH will not be accompanied by a 'background' of 4,5,6-$NADH_3$. The finding that 6-NADH becomes undetectable in mutant U2OS cells complemented with *A. thaliana* PNPO-RP might support this last interpretation if part of the overexpressed enzyme is localised in the mitochondria.

Taken together these findings indicate that PNPO-RP eliminate 6-NADH in yeast, while renalase and to a lesser extent PNPO oxidize 6-NADH in the cytosol of mammalian

cells. The role of PNPO may be dominant in mammalian tissues, like liver, where PNPO is highly expressed while renalase is absent.

Despite significant elevation in the concentration of 4,5,6-$NADH_3$ and presumably of 6-NADH in the absence of 6-NADH metabolizing enzymes, we did not find evidence for metabolic perturbations that would potentially result from inhibition of dehydrogenases such as lactate dehydrogenase by 6-NADH. In the absence of precise knowledge on the concentration of 6-NADH, it is difficult to interpret this lack of effect. Similarly, we do not have explanation to account for the lack of significant effect of PNPO-RP, renalase or PNPO inactivation on the concentration of 6-NADPH or its reduced product 4,5,6-$NADPH_3$.

Connection between the maintenance of pyridine nucleotides and pyridoxal-phosphate

It is very surprising that abnormal pyridine nucleotides are eliminated by members of an enzyme family with a known role in pyridoxal phosphate metabolism. Yet, some evidence suggests that enzymes with a known function in pyridine nucleotide repair are also involved in pyridoxal phosphate metabolism. In bacteria, NADHX epimerase forms a bifunctional protein (called YjeF or Nnr in *E. coli*) with NADHX dehydratase in bacteria (16) and this is not unexpected since bifunctional proteins usually comprise domains with related functions. What is more surprising is that it forms a bifunctional protein with PNPO in Viridiplantae (39,45). This has led to the idea that the epimerase has a second, moonlighting function connected with the metabolism or maintenance of PL5P (46). In support of this hypothesis, the bifunctional protein YjeF clusters with enzymes of pyridoxine synthesis in several bacterial genomes. Furthermore, partial inactivation of a highly conserved lysine in the epimerase domain of YjeF, while causing no detectable increase in NADHX, causes changes in the free PL5P content and other perturbations in the metabolome of *E. coli* (46). The findings in the present paper show yet another connection between nicotinamide nucleotides and PL5P, namely that the same enzyme (PNPO), quite unexpectedly, acts in the maintenance of both cofactors, indicating that despite their structural differences, they may be recognized by the same catalytic site. This indirectly supports the idea that NADHX epimerase may also have a dual specificity by recognizing both pyridoxal phosphate derivatives and pyridine nucleotides.

The wide distribution of 6-NADH oxidase pleads for an important function

As previously stressed, PNPO-RPs are mainly found in photosynthetic organisms, but they are also present in fungi and in scattered species. It would therefore be very interesting to assess whether organisms either have FAD- or FMN-dependent 6-NADH oxidases. Unfortunately, this analysis is not trivial. Despite similarity in 3D structure and function, human and Pseudomonads renalases show only low percentage of sequence identities (24). This makes that it is very difficult to assess the species distribution of 6-NADH oxidases (FAD), though this enzyme seems to be widely distributed.

In any case, the occurrence across evolutionary distant organisms and the existence of two distinct enzymes to catalyze the oxidation of 6-NADH underlines the importance of this process. Curiously, this contrasts with the modest metabolic consequences of the inactivation of 6-NADH oxidases both in human cells and in fungi, possibly due to the fact that 6-NADH is converted to an apparently innocuous ‘super-reduced’ form.

6-NADH and 6-NADPH can form spontaneously. Yet, it is likely that 6-NADH and 6-NADPH may also result from an as yet unknown enzymatic side activity, possibly of a dehydrogenase. Thus, in conditions or cells where the enzyme with this side activity are

highly expressed, the inactivation of 6-NA(P)DH oxidase would likely lead to more dramatic metabolic phenotypes.

In the same line of thought, one may also wonder if primitive dehydrogenases were as specific as the present day enzymes to transfer hydride onto carbon 4 of the nicotinamide moiety of pyridine nucleotides, rather than on C2 or C6. If this has been the case in the early steps of evolution, 6-NADH oxidases may have been then very important to prevent major perturbations of metabolism.

The lack of significant effect of 6-NADH or 4,5,6-$NADH_3$ accumulation on metabolites may be due to several causes, such as the wide variability of metabolite concentration and the fact that statistical analysis has to take into account multiple testing when many metabolites are measured at the same time. However, the main reason for the lack of significant effect is probably that the concentration of 6-NAD(P)H is not high enough to cause significant enzyme inhibition. If it turns out in the future that 6-NADH or 6-NADPH is made by a side activity of an enzyme, overexpressing that enzyme might be a way of inducing metabolic changes related to 6-NAD(P)H accumulation.

Conclusion

Identifying the function of a putative enzyme is a difficult task (47). It is quite remarkable in the present work that the finding of an unexpected-side activity of mouse PNPO led to the identification of what seems to be the physiological function of PNPO-RPs. Exploring the side activities of well characterized proteins may therefore be an interesting avenue to identify enzymes with novel functions, as recently illustrated by the discovery of a new group of microbial lactonases, starting from the side activity of a microbial phosphotriesterase (48).

ACKNOWLEDGEMENTS

We thank Carole L. Linster (University of Luxembourg) and Maria Veiga-da-Cunha (UCLouvain) for helpful discussions; Juliette Létoquart for help in preparing Figure 4.

DECLARATIONS OF INTEREST

The authors declare no conflicts of interest.

FUNDING INFORMATION

This work was supported by the Fonds de la Recherche Scientifique-FRS/FNRS, Walloon Excellence in Life Sciences and Biotechnology (WELBIO), the European Research Council (ERC) under the European Union's Horizon 2020 research and innovation programme grant agreement (No 771704), the Fédération Belge contre le Cancer, UCLouvain and the Loterie Nationale.

AUTHOR CONTRIBUTION STATEMENT

A.Y.M., G.C., G.N., D.V. conducted and analyzed the experiments.
A.Y.M., P.M. G.T.B, and E.V.S designed the experiments.
A.Y.M., G.T.B and E.V.S wrote the paper.

REFERENCES

1. Linster, C. L., Van Schaftingen, E., and Hanson, A. D. (2013) Metabolite damage and its repair or pre-emption. *Nat Chem Biol* **9**, 72-80
2. de Crecy-Lagard, V., Haas, D., and Hanson, A. D. (2018) Newly-discovered enzymes that function in metabolite damage-control. *Curr Opin Chem Biol* **47**, 101-108
3. Peracchi, A. (2018) The Limits of Enzyme Specificity and the Evolution of Metabolism. *Trends Biochem Sci* **43**, 984-996
4. Bommer, G. T., Van Schaftingen, E., and Veiga-da-Cunha, M. (2019) Metabolite repair enzymes control metabolic damage in glycolysis. *Trends in Biochemical Sciences*
5. Lerma-Ortiz, C., Jeffryes, J. G., Cooper, A. J., Niehaus, T. D., Thamm, A. M., Frelin, O., Aunins, T., Fiehn, O., de Crecy-Lagard, V., Henry, C. S., and Hanson, A. D. (2016) 'Nothing of chemistry disappears in biology': the Top 30 damage-prone endogenous metabolites. *Biochem Soc Trans* **44**, 961-971
6. Rzem, R., Veiga-da-Cunha, M., Noel, G., Goffette, S., Nassogne, M. C., Tabarki, B., Scholler, C., Marquardt, T., Vikkula, M., and Van Schaftingen, E. (2004) A gene encoding a putative FAD-dependent L-2-hydroxyglutarate dehydrogenase is mutated in L-2-hydroxyglutaric aciduria. *Proc Natl Acad Sci U S A* **101**, 16849-16854
7. Rzem, R., Achouri, Y., Marbaix, E., Schakman, O., Wiame, E., Marie, S., Gailly, P., Vincent, M. F., Veiga-da-Cunha, M., and Van Schaftingen, E. (2015) A mouse model of L-2-hydroxyglutaric aciduria, a disorder of metabolite repair. *PLoS One* **10**, e0119540
8. Intlekofer, A. M., Dematteo, R. G., Venneti, S., Finley, L. W., Lu, C., Judkins, A. R., Rustenburg, A. S., Grinaway, P. B., Chodera, J. D., Cross, J. R., and Thompson, C. B. (2015) Hypoxia Induces Production of L-2-Hydroxyglutarate. *Cell Metab* **22**, 304-311
9. Collard, F., Baldin, F., Gerin, I., Bolsee, J., Noel, G., Graff, J., Veiga-da-Cunha, M., Stroobant, V., Vertommen, D., Houddane, A., Rider, M. H., Linster, C. L., Van Schaftingen, E., and Bommer, G. T. (2016) A conserved phosphatase destroys toxic glycolytic side products in mammals and yeast. *Nat Chem Biol* **12**, 601-607
10. Segerer, G., Hadamek, K., Zundler, M., Fekete, A., Seifried, A., Mueller, M. J., Koentgen, F., Gessler, M., Jeanclos, E., and Gohla, A. (2016) An essential developmental function for murine phosphoglycolate phosphatase in safeguarding cell proliferation. *Sci Rep* **6**, 35160
11. Veiga-da-Cunha, M., Chevalier, N., Stephenne, X., Defour, J. P., Paczia, N., Ferster, A., Achouri, Y., Dewulf, J. P., Linster, C. L., Bommer, G. T., and Van Schaftingen, E. (2019) Failure to eliminate a phosphorylated glucose analog leads to neutropenia in patients with G6PT and G6PC3 deficiency. *Proc Natl Acad Sci U S A* **116**, 1241-1250
12. Rafter, G. W., Chaykin, S., and Krebs, E. G. (1954) The action of glyceraldehyde-3-phosphate dehydrogenase on reduced diphosphopyridine nucleotide. *J Biol Chem* **2**, 799-811
13. Oppenheimer, N. J., and Kaplan, N. O. (1974) Glyceraldehyde-3-phosphate dehydrogenase catalyzed hydration of the 5-6 double bond of reduced beta-nicotinamide adenine dinucleotide (betaNADH). Formation of beta-6-hydroxy-1,4,5,6-tetrahydronicotinamide adenine dinucleotide. *Biochemistry* **13**, 4685-4694
14. Meinhart, J. O., Chaykin, S., and Krebs, E. G. (1956) Enzymatic conversion of a reduced diphosphopyridine nucleotide derivative to reduced diphosphopyridine nucleotide. *J Biol Chem* **2**, 821-829

15. Acheson, S. A., Kirkman, H. N., and Wolfenden, R. (1988) Equilibrium of 5,6-hydration of NADH and mechanism of ATP-dependent dehydration. *Biochemistry* **27**, 7371-7375
16. Marbaix, A. Y., Noel, G., Detroux, A. M., Vertommen, D., Van Schaftingen, E., and Linster, C. L. (2011) Extremely conserved ATP- or ADP-dependent enzymatic system for nicotinamide nucleotide repair. *J Biol Chem* **286**, 41246-41252
17. Spiegel, R., Shaag, A., Shalev, S., and Elpeleg, O. (2016) Homozygous mutation in the APOA1BP is associated with a lethal infantile leukoencephalopathy. *Neurogenetics* **17**, 187-190
18. Kremer, L. S., Danhauser, K., Herebian, D., Petkovic Ramadza, D., Piekutowska-Abramczuk, D., Seibt, A., Muller-Felber, W., Haack, T. B., Ploski, R., Lohmeier, K., Schneider, D., Klee, D., Rokicki, D., Mayatepek, E., Strom, T. M., Meitinger, T., Klopstock, T., Pronicka, E., Mayr, J. A., Baric, I., Distelmaier, F., and Prokisch, H. (2016) NAXE Mutations Disrupt the Cellular NAD(P)HX Repair System and Cause a Lethal Neurometabolic Disorder of Early Childhood. *Am J Hum Genet* **99**, 894-902
19. Van Bergen, N. J., Guo, Y., Rankin, J., Paczia, N., Becker-Kettern, J., Kremer, L. S., Pyle, A., Conrotte, J.-F., Ellaway, C., Procopis, P., Prelog, K., Homfray, T., Baptista, J., Baple, E., Wakeling, M., Massey, S., Kay, D. P., Shukla, A., Girisha, K. M., Lewis, L. E. S., Santra, S., Power, R., Daubeney, P., Montoya, J., Ruiz-Pesini, E., Kovacs-Nagy, R., Pritsch, M., Ahting, U., Thorburn, D. R., Prokisch, H., Taylor, R. W., Christodoulou, J., Linster, C. L., Ellard, S., and Hakonarson, H. (2019) NAD(P)HX dehydratase (NAXD) deficiency: a novel neurodegenerative disorder exacerbated by febrile illnesses. *Brain* **142**, 50-58
20. Becker-Kettern, J., Paczia, N., Conrotte, J. F., Zhu, C., Fiehn, O., Jung, P. P., Steinmetz, L. M., and Linster, C. L. (2018) NAD(P)HX repair deficiency causes central metabolic perturbations in yeast and human cells. *FEBS J* **285**, 3376-3401
21. Godtfredsen, S. E., and Ottesen, M. (1978) 1,6-dihydro-NAD as an humidity-induced lactate dehydrogenase inhibitor in NADH preparations. *Carlsberg Res. Commun.* **43**, 171-175
22. Godtfredsen, S. E., and Ottesen, M. (1979) On the mode of formation of 1,6-dihydro-NAD in NADH preparations. *Carlsberg Res. Commun.* **44**, 65-75
23. Beaupre, B. A., Hoag, M. R., Roman, J., Forsterling, F. H., and Moran, G. R. (2015) Metabolic function for human renalase: oxidation of isomeric forms of beta-NAD(P)H that are inhibitory to primary metabolism. *Biochemistry* **54**, 795-806
24. Hoag, M. R., Roman, J., Beaupre, B. A., Silvaggi, N. R., and Moran, G. R. (2015) Bacterial Renalase: Structure and Kinetics of an Enzyme with 2- and 6-Dihydro-beta-NAD(P) Oxidase Activity from Pseudomonas phaseolicola. *Biochemistry* **54**, 3791-3802
25. Moran, G. R. (2016) The catalytic function of renalase: A decade of phantoms. *Biochim Biophys Acta* **1864**, 177-186
26. Moran, G. R., and Hoag, M. R. (2017) The enzyme: Renalase. *Arch Biochem Biophys* **632**, 66-76
27. Veiga-da-Cunha, M., Chevalier, N., Stroobant, V., Vertommen, D., and Van Schaftingen, E. (2014) Metabolite proofreading in carnosine and homocarnosine synthesis: molecular identification of PM20D2 as beta-alanyl-lysine dipeptidase. *J Biol Chem* **289**, 19726-19736
28. Arts, I. S., Ball, G., Leverrier, P., Garvis, S., Nicolaes, V., Vertommen, D., Ize, B., Tamu Dufe, V., Messens, J., Voulhoux, R., and Collet, J. F. (2013) Dissecting the machinery that introduces disulfide bonds in Pseudomonas aeruginosa. *MBio* **4**, e00912-00913

29. Emanuelsson, O., Nielsen, H., Brunak, S., and von Heijne, G. (2000) Predicting subcellular localization of proteins based on their N-terminal amino acid sequence. *J Mol Biol* **300**, 1005-1016
30. Kitagawa, M., Ara, T., Arifuzzaman, M., Ioka-Nakamichi, T., Inamoto, E., Toyonaga, H., and Mori, H. (2005) Complete set of ORF clones of Escherichia coli ASKA library (a complete set of E. coli K-12 ORF archive): unique resources for biological research. *DNA Res* **12**, 291-299
31. Musayev, F. N., Di Salvo, M. L., Ko, T. P., Schirch, V., and Safo, M. K. (2003) Structure and properties of recombinant human pyridoxine 5'-phosphate oxidase. *Protein Sci* **12**, 1455-1463
32. Goldstein, A. L., and McCusker, J. H. (1999) Three new dominant drug resistance cassettes for gene disruption inSaccharomyces cerevisiae. *Yeast* **15**, 1541-1553
33. Gietz, R. D., and Schiestl, R. H. (2007) High-efficiency yeast transformation using the LiAc/SS carrier DNA/PEG method. *Nat Protoc* **2**, 31-34
34. Milani, M., Ciriello, F., Baroni, S., Pandini, V., Canevari, G., Bolognesi, M., and Aliverti, A. (2011) FAD-Binding Site and NADP Reactivity in Human Renalase: A New Enzyme Involved in Blood Pressure Regulation. *Journal of Molecular Biology* **411**, 463-473
35. Lorenz, M. A., Burant, C. F., and Kennedy, R. T. (2011) Reducing time and increasing sensitivity in sample preparation for adherent mammalian cell metabolomics. *Anal Chem* **83**, 3406-3414
36. Merrill, A. H., Horiike, K., and McCormick, D. B. (1978) Evidence for the regulation of pyridoxal 5′-phosphate formation in liver by pyridoxamine (pyridoxine) 5′-phosphate oxidase. *Biochemical and Biophysical Research Communications* **83**, 984-990
37. Naylor, C. E., Gover, S., Basak, A. K., Cosgrove, M. S., Levy, H. R., and Adams, M. J. (2001) NADP+ and NAD+ binding to the dual coenzyme specific enzyme Leuconostoc mesenteroides glucose 6-phosphate dehydrogenase: different interdomain hinge angles are seen in different binary and ternary complexes. *Acta Crystallogr D Biol Crystallogr* **57**, 635-648
38. Tsuge, H., Sen-Maru, K., and Ohashi, K. (1978) Immobilization of yeast pyridoxamine (pyridoxine) 5′-phosphate oxidase by organomercurial agarose. *FEBS Letters* **93**, 331-334
39. Sang, Y., Barbosa, J. M., Wu, H., Locy, R. D., and Singh, N. K. (2007) Identification of a pyridoxine (pyridoxamine) 5'-phosphate oxidase from Arabidopsis thaliana. *FEBS Lett* **581**, 344-348
40. Di Salvo, M., Yang, E., Zhao, G., Winkler, M. E., and Schirch, V. (1998) Expression, purification, and characterization of recombinant Escherichia coli pyridoxine 5'-phosphate oxidase. *Protein Expr Purif* **13**, 349-356
41. Sang, Y., Goertzen, L. R., Tzou, Y.-M., Locy, R. D., and Singh, N. K. (2010) Identification of a second pyridoxine (pyridoxamine) 5′-phosphate oxidase in Arabidopsis thaliana. *Acta Physiologiae Plantarum* **33**, 559-566
42. di Salvo, M. L., Safo, M. K., Musayev, F. N., Bossa, F., and Schirch, V. (2003) Structure and mechanism of Escherichia coli pyridoxine 5′-phosphate oxidase. *Biochimica et Biophysica Acta (BBA) - Proteins and Proteomics* **1647**, 76-82
43. Chakraverty, K., and Chaykin, S. (1964) 1,6 DPNH, an enzymatically active form of reduced DPN. *Biochemical and Biophysical Research Communications* **15**, 262-268
44. Lui, A., Lumeng, L., and Li, T. K. (1981) Metabolism of vitamin B6 in rat liver mitochondria. *J. Biol. Chem.* **256**, 6041-6046

45. Niehaus, T. D., Richardson, L. G., Gidda, S. K., ElBadawi-Sidhu, M., Meissen, J. K., Mullen, R. T., Fiehn, O., and Hanson, A. D. (2014) Plants utilize a highly conserved system for repair of NADH and NADPH hydrates. *Plant Physiol* **165**, 52-61
46. Niehaus, T. D., Elbadawi-Sidhu, M., Huang, L., Prunetti, L., Gregory, J. F., 3rd, de Crecy-Lagard, V., Fiehn, O., and Hanson, A. D. (2018) Evidence that the metabolite repair enzyme NAD(P)HX epimerase has a moonlighting function. *Biosci Rep* **38**
47. Ellens, K. W., Christian, N., Singh, C., Satagopam, V. P., May, P., and Linster, C. L. (2017) Confronting the catalytic dark matter encoded by sequenced genomes. *Nucleic Acids Res* **45**, 11495-11514
48. Afriat, L., Roodveldt, C., Manco, G., and Tawfik, D. S. (2006) The latent promiscuity of newly identified microbial lactonases is linked to a recently diverged phosphotriesterase. *Biochemistry* **45**, 13677-13686

TABLE 1

	6-NADH			6-NADPH			2-NADH			PM5P			PN5P		
Protein and specie	K_M (µM)	V_{max} (µmole /min/ mg)	k_{cat}/K_M (s^{-1} . mM^{-1})	K_M (µM)	V_{max} (µmole /min/ mg)	k_{cat}/K_M (s^{-1} . mM^{-1})	K_M (µM)	V_{max} (µmole /min/ mg)	k_{cat}/K_M (s^{-1} . mM^{-1})	K_M (µM)	V_{max} (µmole /min/ mg)	k_{cat}/K_M (s^{-1} . mM^{-1})	K_M (µM)	V_{max} (µmole /min/ mg)	k_{cat}/K_M (s^{-1} . mM^{-1})
Pnpo ***M. musculus***	25.5 ± 1.4	0.5 ± 0.0	**8.9**	4.2 ± 0.3	0.8 ± 0.0	**82.8**	59.6 ± 5.5	0.4 ± 0.0	**2.7**	< 1.0 ± 0.1	0.1 ± 0.0	**> 52**	< 1.0 ± 0.1	0.2 ± 0.0	**> 102**
Pdx3 ***S. cerevisiae***	159.3 ± 9.2	0.2 ± 0.0	**0.6**	5.8 ± 0.9	0.04 ± 0.00	**3.1**	N.A	N.A.	N.A.	32.1 ± 4.5	0.2 ± 0.0	**2.4**	3.3 ± 0.7	0.05 ± 0.00	**6.4**
PdxH ***E. coli***	264 ± 49	0.4 ± 0.0	**0.7**	30.7 ± 4.4	0.1 ± 0.0	**1.85**	N.A	N.A.	N.A.	91.2 ± 8.1	0.1 ± 0.0	**0.7**	1.9 ± 0.3	0.1 ± 0.0	**31.4**
PPOX															

Table 1: Kinetic properties of different pyridoxamine-phosphate oxidases on their classical substrates pyridoxine- and pyridoxamine-phosphate and on 2-NADH, 6-NADH and 6-NADPH. 6-NADH and 6-NADPH oxidase activities of recombinant PNPOs from *M. musculus*, *S. cerevisiae*, *E. coli* and *A. thaliana* were assayed in a mixture at pH 7.1 by following the decrease of absorbance at 345 nm. 2-NADH oxidase activity was assayed under the same conditions by following the decrease in absorbance at 395 nm. Pyridoxine- and pyridoxamine-phosphate oxidase activities of the same proteins were assayed in a mixture at pH 8.5 containing 200 mM of Tris buffer. The formation of the Tris-PL5P complex was followed at 414 nm (31). K_M and V_{max} were calculated with the Prism software. N.T. : not tested. N.A. : no activity. As mentioned in the Experimental section, the V_{max} and k_{cat}/K_M values are somewhat underestimated, due to difficulties in measuring the precise enzyme concentration.

TABLE 2

		6-NADH			6-NADPH			2-NADH		
Specie	Prot	K_M (µM)	V_{max} (µmole/ min/mg)	k_{cat}/K_M ($s^{-1}.mM^{-1}$)	K_M (µM)	V_{max} (µmole/ min/mg)	k_{cat}/K_M ($s^{-1}.mM^{-1}$)	K_M (µM)	V_{max} (µmole/ min/mg)	k_{cat}/K_M ($s^{-1}.mM^{-1}$)
A. thaliana	**AtPPOX2**	< 1.0 ± 0.2	0.6 ± 0.0	**> 259**	2.6 ± 0.8	0.7 ± 0.05	**125**	1.6 ± 0.5	0.4 ± 0.0	**125**
S. cerevisiae	**Ygr017w**	4.7 ± 0.7	0.6 ± 0.0	**85**	4.1 ± 0.6	1.1 ± 0.05	**168**	3.3 ± 0.5	0.2 ± 0.0	**31**
N. Punctiforme	**NpPPOX2**	4.8 ± 0.7	3.9 ± 0.1	**331**	15.6 ± 2.7	5.9 ± 0.3	**158**	< 1.0± 0.2	0.9 ± 0.0	**> 396**
H. Sapiens	**RNLS**	12.2± 2.2	0.9 ± 0.1	**54**	1.0 ± 0.2	0.4 ± 0.0	**287**	9.7± 1.1	0.2 ± 0.0	**12**

Table 2: Kinetic properties of pyridoxamine-phosphate-oxidase-related proteins from different species and of Renalase for 6-NADH, 6-NADPH and 2-NADH. 6-NADH, 6-NADPH and 2-NADH oxidase activities of recombinant PNPO-RPs from *A. thaliana* (PPOX2), *S. cerevisiae* (Ygr017w) and *Nostoc punctiforme* (NpPPOX2) as well as those of recombinant renalase from *Homo sapiens* (RNLS) were assayed in a mixture at pH 7.1 by following the decrease of absorbance at 345 nm (6-NAD(P)H) or at 395 nm (2-NADH). 2-NADPH was too unstable to be tested. No activity could be detected on pyridoxine- or pyridoxamine-phosphate (tested at 25 µM). Same remark as in Table 1 on the underestimation of V_{max} and k_{cat}/K_M values.

FIGURES

Figure 1: Formation and metabolism of 2- and 6-NAD(P)H. Spontaneous hydride transfer from NAD(P)H to $NAD(P)^+$ leads to the formation of 2- and 6-NAD(P)H. 6-NAD(P)H, a strong inhibitor of several dehydrogenases, can be further reduced to 4,5,6-$NAD(P)H_3$ by glyceraldehyde-3-phosphate dehydrogenase (GAPDH) or glucose-6-phosphate dehydrogenase (G6PDH) in the presence of the appropriate substrate. Renalase (RNLS) and, as shown in the present work, PNPO and PNPO-RP catalyse the oxidation of 2- and 6-NAD(P)H.

Figure 2: Elution profile of 6-NADPH oxidase and pyridoxamine-phosphate (PM5P) oxidase activities from a DEAE-Sepharose column. A rat liver extract was applied on a DEAE-Sepharose column as described in the Experimental section. Proteins were eluted with a salt gradient and fractions of 5 ml were collected. Both 6-NADPH consumption (red squares) and pyridoxamine-phosphate oxidase (green triangles) were assayed. Black circles represent A_{280}.

Figure 3: Alignment of pyridoxamine-phosphate oxidases with different PNPO-RPs. The sequences of PNPO from *S. cerevisiae* (PNPOSc, Pdx3, NP_009591.1), *E. coli* (PNPOEc, PdxH, WP_001282319.1), *M. musculus* (PNPOMm, NP_598782.1; from residue 11), and *A. thaliana* (PNPOAt, PPOX1, NP_568717.2, from residue 315) were aligned with PNPO-RP from *S. cerevisiae* (PNPO-RPSc, Ygr017w, NP_011531.1), *A. thaliana* (PNPO-RPAt, AtPPOX2, NP_566081.1) and *N. punctiforme* (PNPO-RPNp, NpPPOX2 WP_012411992.1) with Clustal Omega. Residues conserved in all proteins are highlighted in cyan, while residues conserved only in PNPOs or in PNPO-RPs are highlighted in grey and yellow, respectively. Conserved residues that surround the putative catalytic site in PNPO-RPs are bold and underlined. The inserts naturally present in the *S. cerevisiae* PNPO-RP are in red type.

Figure 4: Structure of the catalytic site of *Nostoc punctiforme* PNPO-RP.
The figure shows one of the two FMNs of the dimer. As in Fig. 3, conserved residues in both PNPO and PNPO-RP are shown in cyan, while the PNPO-RP specific residues are shown in yellow. Numbering indicates the residues belonging to chain A or B. The structure reported in pdb under accession 2i51 has been deposited by the Joint Center for Structural Genomics (JCSG). The figure has been drawn with MacPyMol.

Figure 5: Reduction of 6-NADH and 6-NADPH by dehydrogenases to hypothetical 4,5,6-$NAD(P)H_3$
A & B. Spectrophotometric assays showing the reduction of 6-NADH (≈ 50 µM) by *Sus scrofa* glyceraldehyde-3-phosphate dehydrogenase (GAPDH; 0.25 mg/ml) in the presence of 0.5 mM glyceraldehyde-3-phosphate (GAP) (A) and of 6-NADPH (≈ 50 µM) by *L. mesenteroïdes* glucose-6-phosphate dehydrogenase (G6PDH; 40 U/ml) in the presence of 0.8 mM glucose-6-phosphate (G6P) (B). Reduction was carried out for 5 and 30 min, as indicated. Controls without GAP or G6P are also shown (dotted line). C. LC-MS analysis of the reduction of 6-NADH to 4,5,6-$NADH_3$ by *S. scrofa* GAPDH in the presence of glyceraldehyde-3-phosphate (GAP). 25 µM 6-NADH was incubated at 30°C in a mix containing 25 mM Hepes, pH 7.1, 20 mM KCl, 1 mM $MgCl_2$, 0.1 mg/ml BSA, 5 mM potassium arsenate, 0.2 mg/ml pig GAPDH with or without 0.5 mM glyceraldehyde 3-phosphate during 0 and 45 min. 10 µl of the mixture was diluted 10-fold in a 90%

$MeOH/CHCl_3$ (9/1) solution and a 5 µl sample was analysed by LC-MS. Left and right panels show the detected signals for m/z 664.1177 and 666.1332, corresponding to 6-NADH and 4,5,6-$NADH_3$, respectively. The resolution used during the LC-MS analysis (10 ppm) allowed us to distinguish 6-NADH with 2 ^{13}C (m/z 666.122) from 4,5,6-$NADH_3$ (m/z 666.133) D. Spectra of 4,5,6-$NADH_3$ (orange), (S)-NADHX (red), 6-NADH (green) and NADH (blue) and structures of 4,5,6-$NADH_3$ and (S)-NADHX.

Figure 6 : Q-PCR analysis of the expression of PNPO and Renalase in mouse tissues. RT-qPCR was performed with cDNA from 9 different tissues. Expression was normalised to TATA Binding Protein (TBP) mRNA expression using the 2^{-dCt} method. The values shown are means ± SD for three different mice. Sk. Muscle : Skeletal muscle.

Figure 7 : Effect of inactivation of the PNPO and Renalase genes on the amount of pyridoxine-5'-P, 6-NADH and 4,5,6-$NADH_3$ in U2OS cells.
A-C. Wild type (WT) cells, two different clones of the single mutants (ΔPNPO1 or 2; Δ RNLS1 or 2) and two different clones of the double mutant (ΔPNPO/ΔRNLS 1 or 2) were analysed by LC/MS. D-F. Wild type and clones ΔPNPO/ΔRNLS 1 and 2 (DKO1 and DKO2) complemented or not with human PNPO (PNPO), human renalase (RNLS), both of them (PNPO + RNLS) or A. thaliana PNPO-RP (PNPO-RP) were also analysed. Pyridoxine-5'-P (A and D), 6-NADH (B and E) and 4,5,6-$NADH_3$ (C and F) were quantified. The peaks obtained by LC-MS were divided by the Total Ion Current (TIC) of the chromatogram. Means ± SEM for $n \geq 3$. Statistical analyses were performed by student t-test.

Figure 8 : Effect of inactivation of the yeast PNPO (Pdx3) and PNPO-RP (Ygr017w) genes on the amount of pyridoxine-5'-P, 6-NADH and 4,5,6-$NADH_3$. Wild-type (WT), PNPO single knockout (pdx3Δ), PNPO-RP single knockout (ygr017wΔ) and double knockout pdx3Δygr017wΔ) yeast cells were grown in minimal medium containing 25 µM pyridoxal until OD_{600} reached ≈ 1 to 1.5. Cells were quenched and metabolites were extracted and analysed as described in experimental procedures. Pyridoxine-5'-P (A), 6-NADH (B) and 4,5,6-$NADH_3$ (C) were quantified. The peaks obtained by LC-MS were divided by the Total Ion Current (TIC) of the chromatogram. Means ± SEM for $n \geq 3$. Statistical analyses were performed by student t-test.

Figure 1

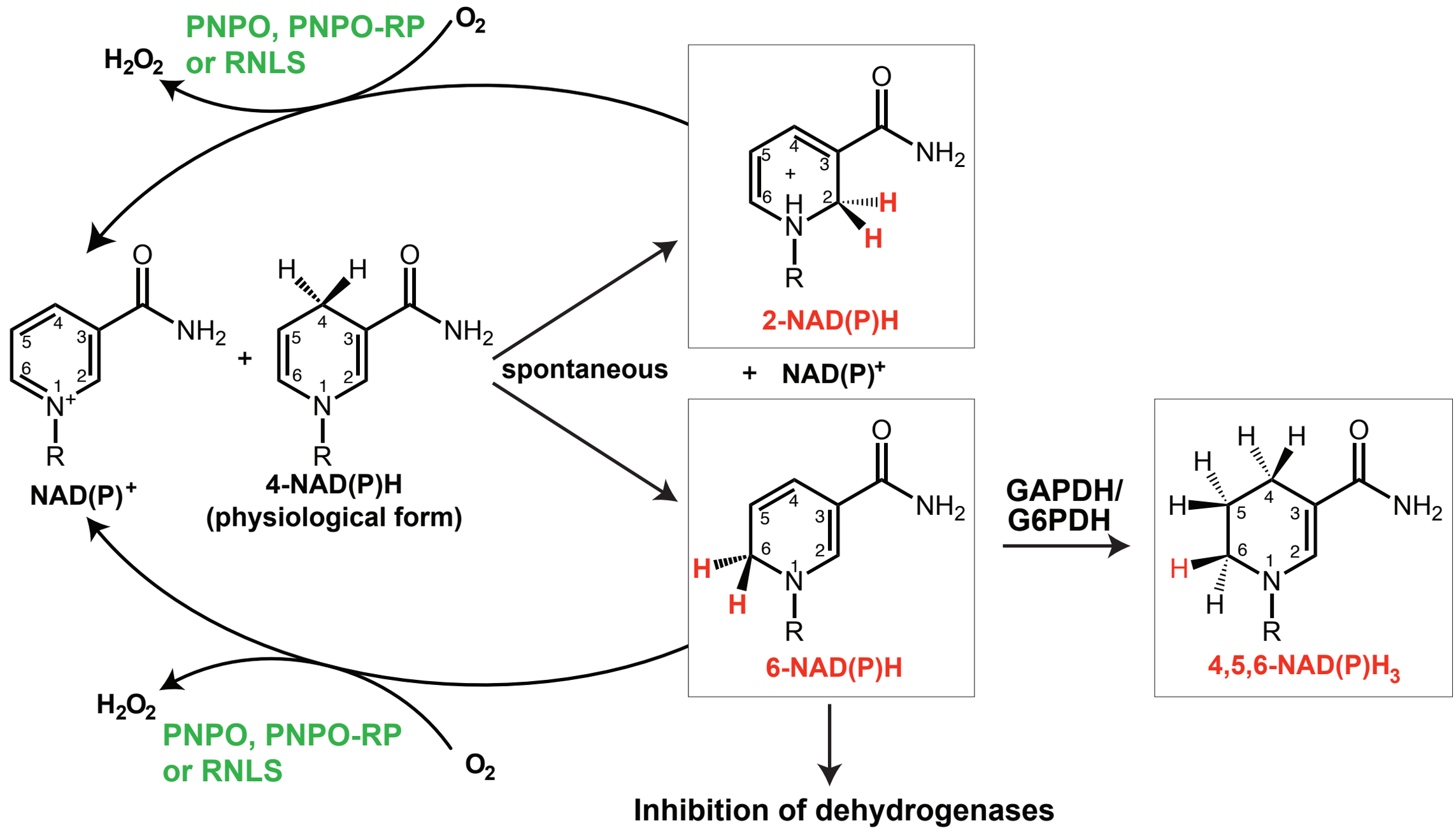
PNPO, PNPO-RP
or RNLS
O_2
H_2O_2
NAD(P)+
4-NAD(P)H
(physiological form)
spontaneous
2-NAD(P)H
+ NAD(P)+
6-NAD(P)H
GAPDH/
G6PDH
4,5,6-NAD(P)H3
H_2O_2
PNPO, PNPO-RP
or RNLS
O_2
Inhibition of dehydrogenases

Figure 2

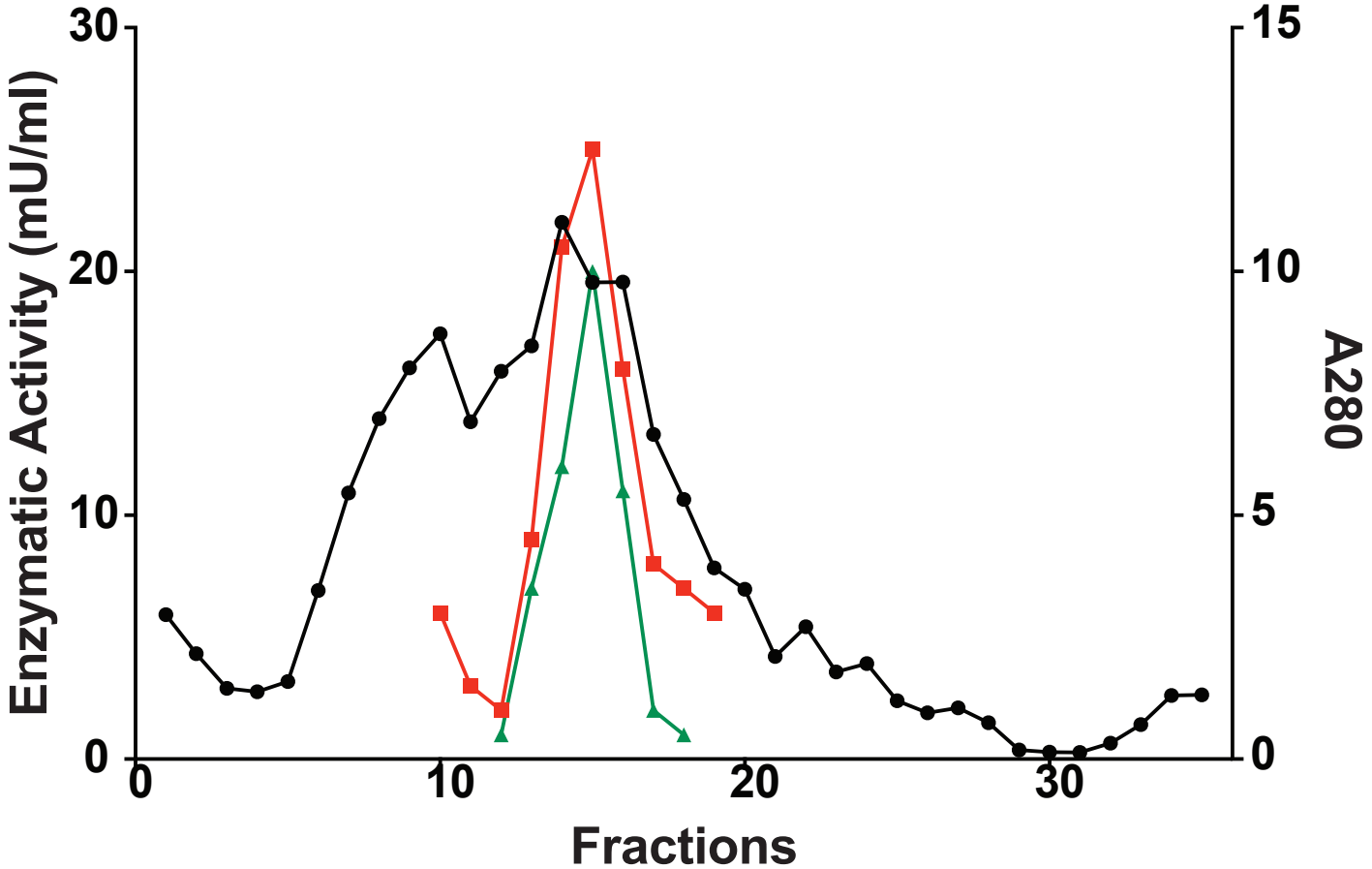
30
20
10
0
Enzymatic Activity (mU/ml)
15
10
5
0
A280
0
10
20
30
Fractions

Figure 3

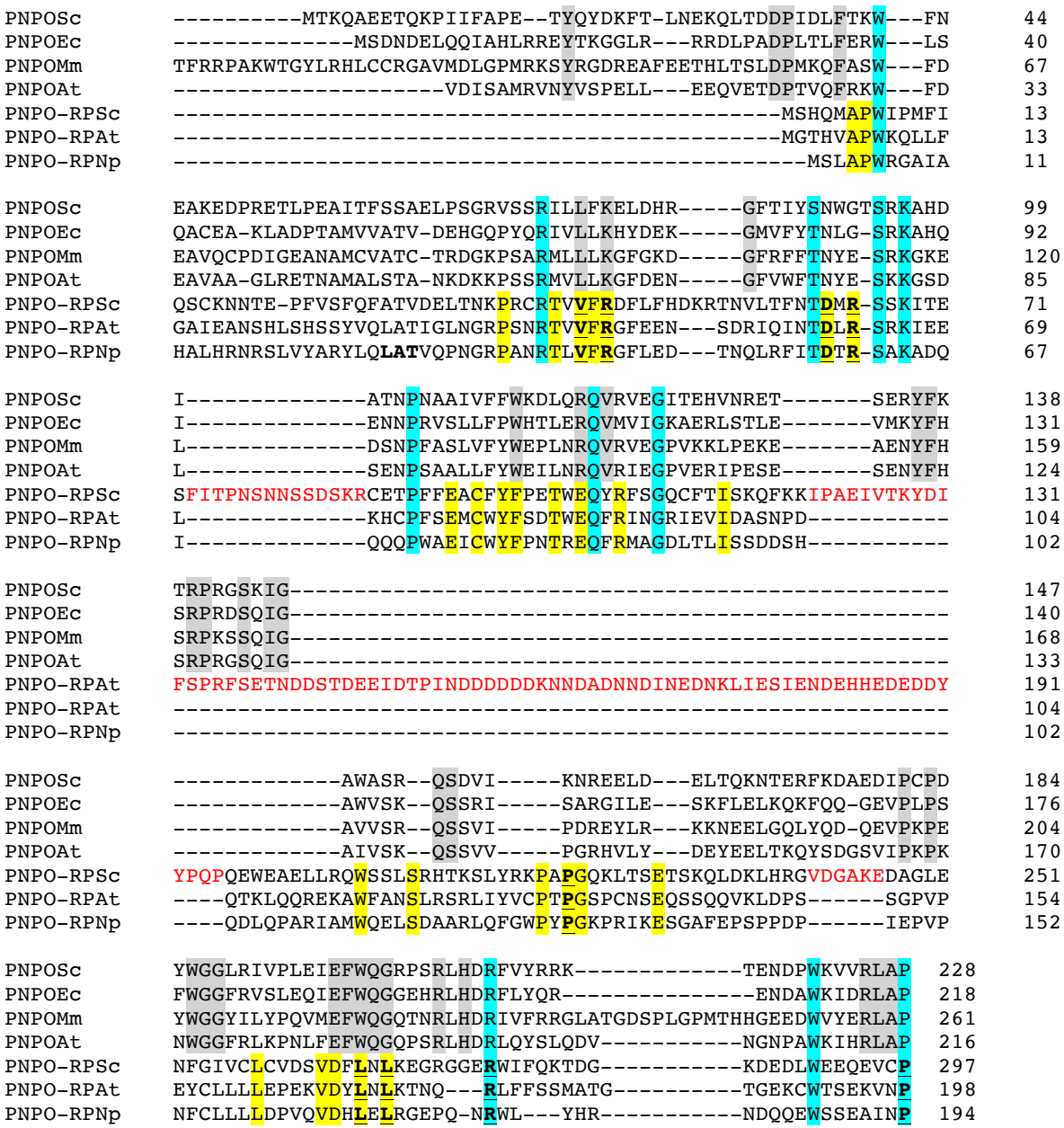
PNPOSc ----------MTKQAEETQKPIIFAPE--TYQYDKFT-LNEKQLTDDPIDLFTKW---FN 44
PNPOEc --------------MSDNDELQQIAHLRREYTKGGLR---RRDLPADPLTLFERW---LS 40
PNPOMm TFRRPAKWTGYLRHLCCRGAVMDLGPMRKSYRGDREAFEETHLTSLDPMKQFASW---FD 67
PNPOAt ----------------------VDISAMRVNYVSPELL---EEQVETDPTVQFRKW---FD 33
PNPO-RPSc --MSHQMAPWIPMFI 13
PNPO-RPAt --MGTHVAPWKQLLF 13
PNPO-RPNp --MSLAPWRGAIA 11
PNPOSc EAKEDPRETLPEAITFSSAELPSGRVSSRILLFKELDHR-----GFTIYSNWGTSRKAHD 99
PNPOEc QACEA-KLADPTAMVVATV-DEHGQPYQRIVLLKHYDEK-----GMVFYTNLG-SRKAHQ 92
PNPOMm EAVQCPDIGEANAMCVATC-TRDGKPSARMLLLKGFGKD-----GFRFFTNYE-SRKGKE 120
PNPOAt EAVAA-GLRETNAMALSTA-NKDKKPSSRMVLLKGFDEN-----GFVWFTNYE-SKKGSD 85
PNPO-RPSc QSCKNNTE-PFVSFQFATVDELTNKPRCRTVVFRDFLFHDKRTNVLTFNTDMR-SSKITE 71
PNPO-RPAt GAIEANSHLSHSSYVQLATIGLNGRPSNRTVVFRGFEEN---SDRIQINTDLR-SRKIEE 69
PNPO-RPNp HALHRNRSLVYARYLQLATVQPNGRPANRTLVFRGFLED---TNQLRFITDTR-SAKADQ 67
PNPOSc I--------------ATNPNAAIVFFWKDLQRQVRVEGITEHVNRET-------SERYFK 138
PNPOEc I--------------ENNPRVSLLFPWHTLERQVMVIGKAERLSTLE-------VMKYFH 131
PNPOMm L--------------DSNPFASLVFYWEPLNRQVRVEGPVKKLPEKE-------AENYFH 159
PNPOAt L--------------SENPSAALLFYWEILNRQVRIEGPVERIPESE-------SENYFH 124
PNPO-RPSc SFITPNSNNSSDSKRCETPFFEACFYFPETWEQYRFSGQCFTISKQFKKIPAEIVTKYDI 131
PNPO-RPAt L--------------KHCPFSEMCWYFSDTWEQFRINGRIEVIDASNPD---------- 104
PNPO-RPNp I--------------QQQPWAEICWYFPNTREQFRMAGDLTLISSDDSH---------- 102
PNPOSc TRPRGSKIG---------- 147
PNPOEc SRPRDSQIG---------- 140
PNPOMm SRPKSSQIG---------- 168
PNPOAt SRPRGSQIG---------- 133
PNPO-RPAt FSPRFSETNDDSTDEEIDTPINDDDDDDKNNDADNNDINEDNKLIESIENDEHHEDEDDY 191
PNPO-RPAt ---------- 104
PNPO-RPNp ---------- 102
PNPOSc -------------AWASR--QSDVI-----KNREELD---ELTQKNTERFKDAEDIPCPD 184
PNPOEc -------------AWVSK--QSSRI-----SARGILE---SKFLELKQKFQQ-GEVPLPS 176
PNPOMm -------------AVVSR--QSSVI-----PDREYLR---KKNEELGQLYQD-QEVPKPE 204
PNPOAt -------------AIVSK--QSSVV-----PGRHVLY---DEYEELTKQYSDGSVIPKPK 170
PNPO-RPSc YPQPQEWEAELLRQWSSLSRHTKSLYRKPAPGQKLTSETSKQLDKLHRGVDGAKEDAGLE 251
PNPO-RPAt ----QTKLQQREKAWFANSLRSRLIYVCPTPGSPCNSEQSSQQVKLDPS------SGPVP 154
PNPO-RPNp ----QDLQPARIAMWQELSDAARLQFGWPYPGKPRIKESGAFEPSPPDP------IEPVP 152
PNPOSc YWGGLRIVPLEIEFWQGRPSRLHDRFVYRRK----------TENDPWKVVRLAP 228
PNPOEc FWGGFRVSLEQIEFWQGGEHRLHDRFLYQR----------ENDAWKIDRLAP 218
PNPOMm YWGGYILYPQVMEFWQGQTNRLHDRIVFRRGLATGDSPLGPMTHHGEEDWVYERLAP 261
PNPOAt NWGGFRLKPNLFEFWQGQPSRLHDRLQYSLQDV----------NGNPAWKIHRLAP 216
PNPO-RPSc NFGIVCLCVDSVDFLNLKEGRGGERWIFQKTDG----------KDEDLWEEQEVCP 297
PNPO-RPAt EYCLLLLEPEKVDYLNLKTNQ---RLFFSSMATG----------TGEKCWTSEKVNP 198
PNPO-RPNp NFCLLLLDPVQVDHLELRGEPQ-NRWL---YHR----------NDQQEWSSEAINP 194

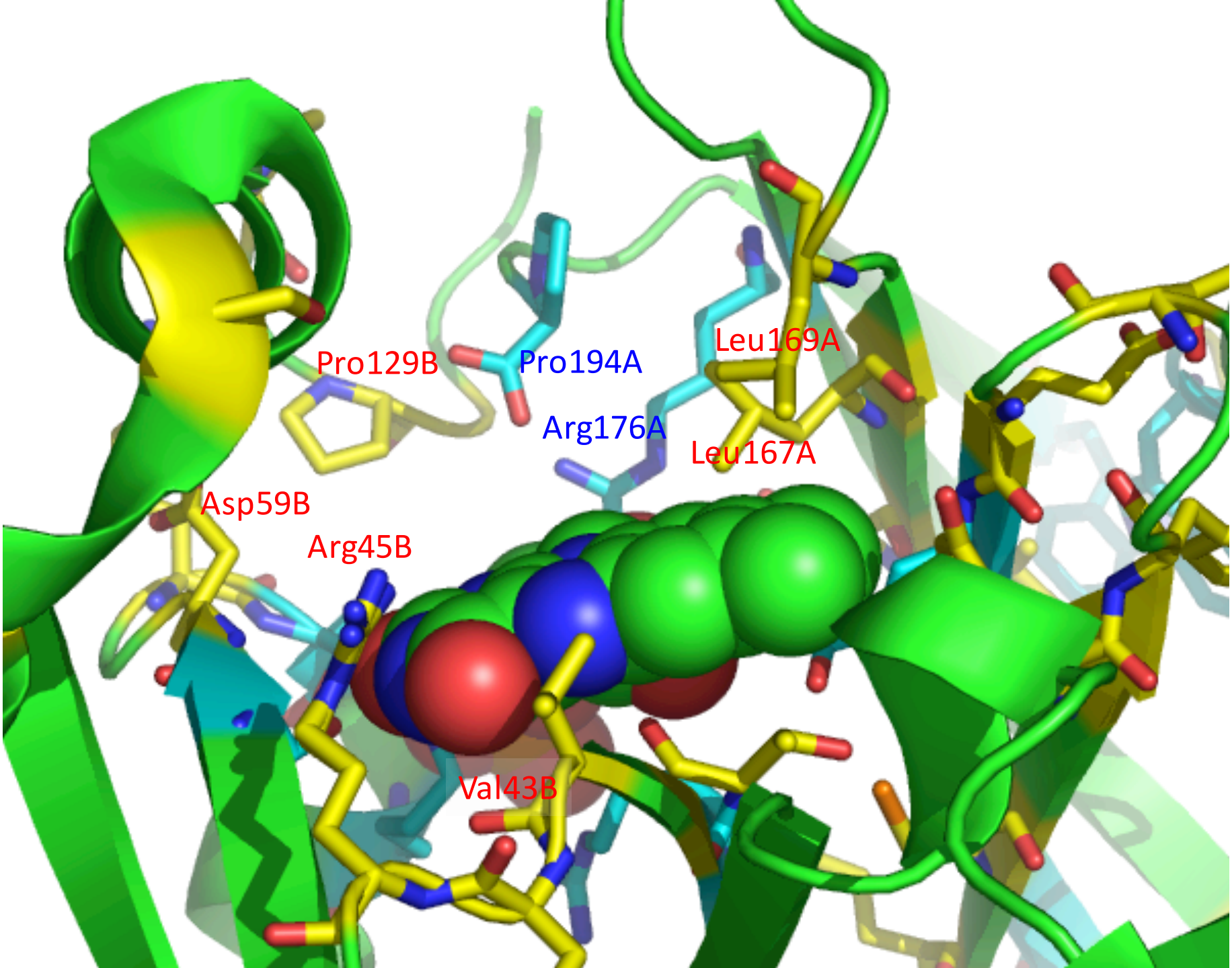
Pro129B
Pro194A
Leu169A
Arg176A
Leu167A
Asp59B
Arg45B
Val43B

Figure 5

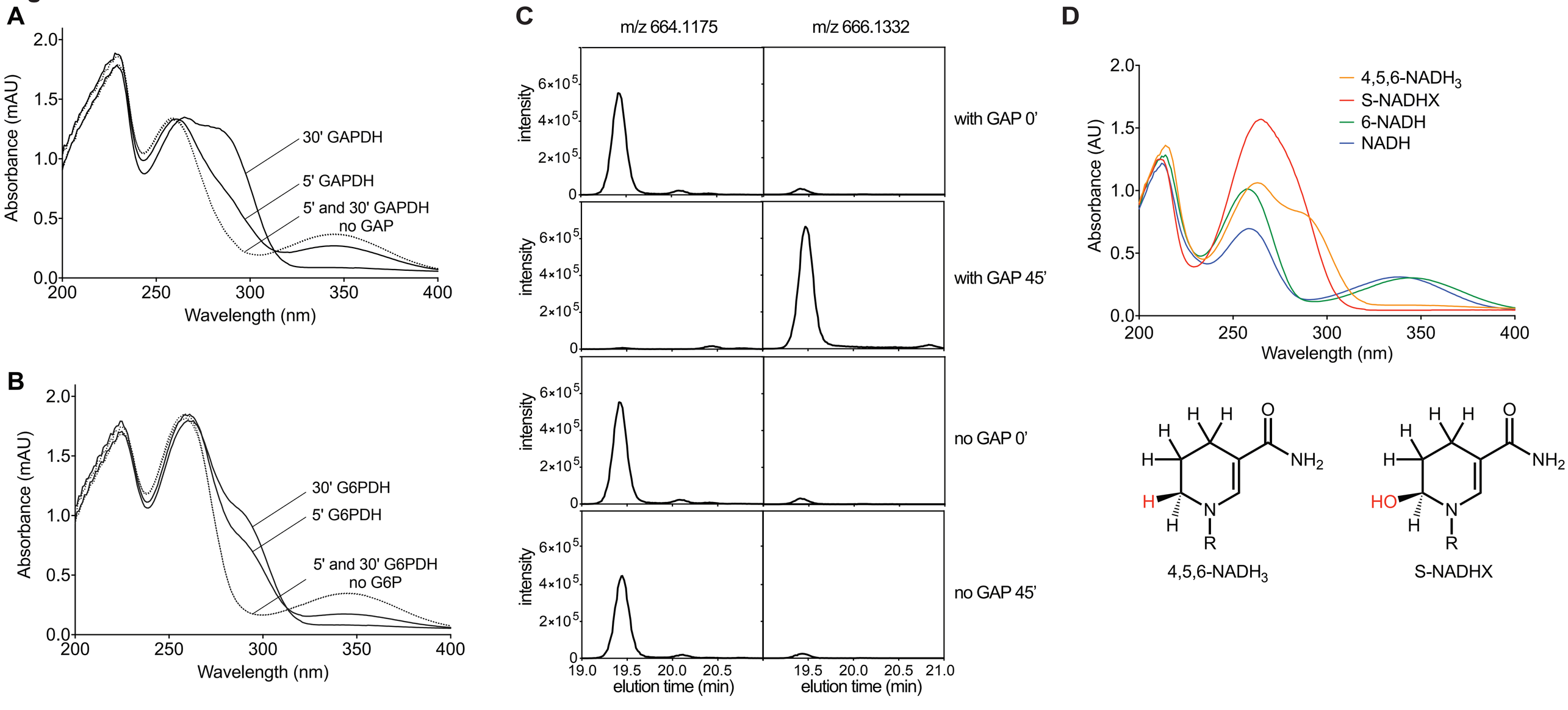
A
Absorbance (mAU)
Wavelength (nm)
30' GAPDH
5' GAPDH
5' and 30' GAPDH
no GAP
B
Absorbance (mAU)
Wavelength (nm)
30' G6PDH
5' G6PDH
5' and 30' G6PDH
no G6P
C
m/z 664.1175
m/z 666.1332
intensity
with GAP 0'
with GAP 45'
no GAP 0'
no GAP 45'
elution time (min)
D
Absorbance (AU)
Wavelength (nm)
4,5,6-NADH3
S-NADHX
6-NADH
NADH
4,5,6-NADH3
S-NADHX

Figure 6

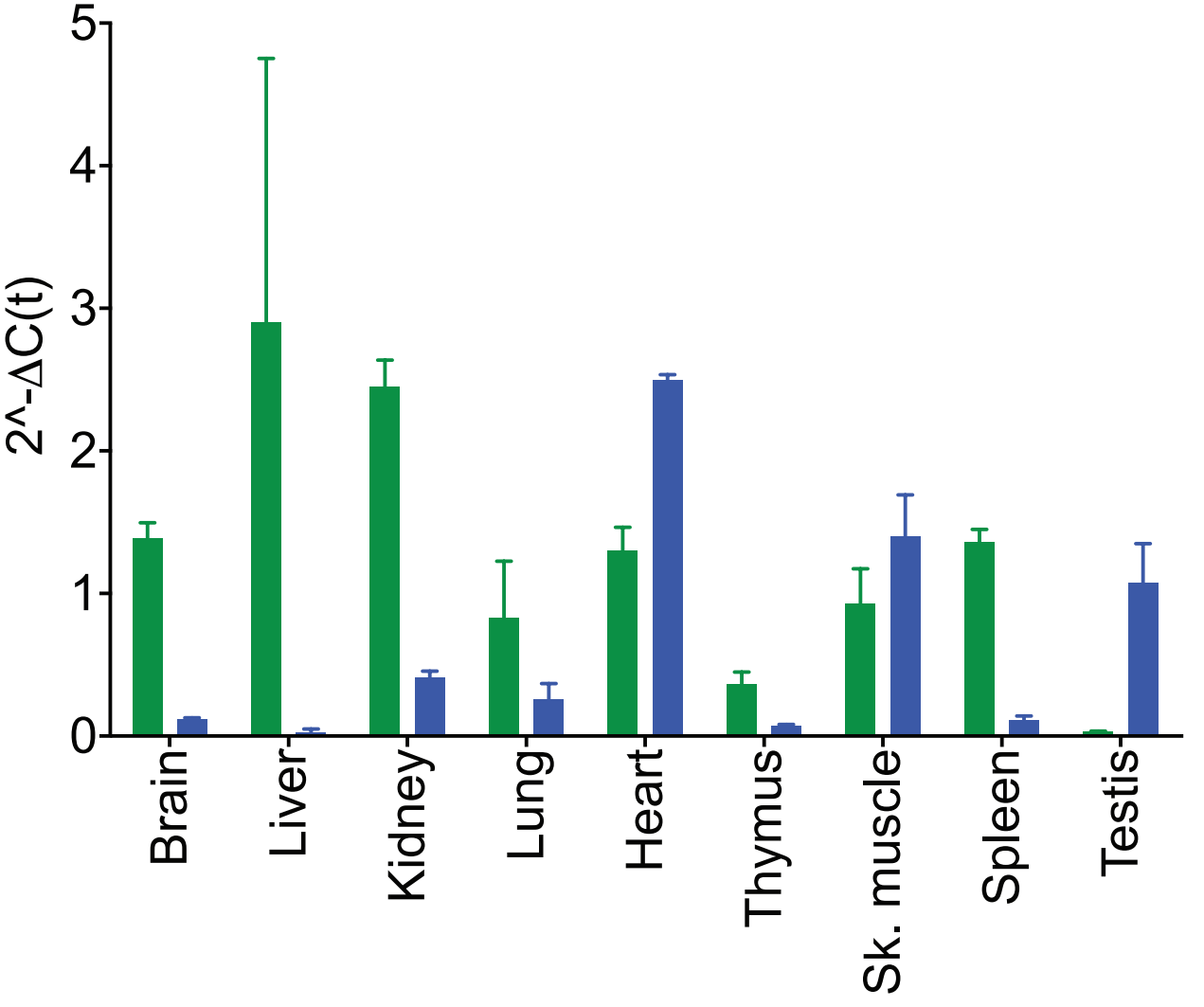
2^-ΔC(t)
5
4
3
2
1
0
Brain
Liver
Kidney
Lung
Heart
Thymus
Sk. muscle
Spleen
Testis

Figure 7

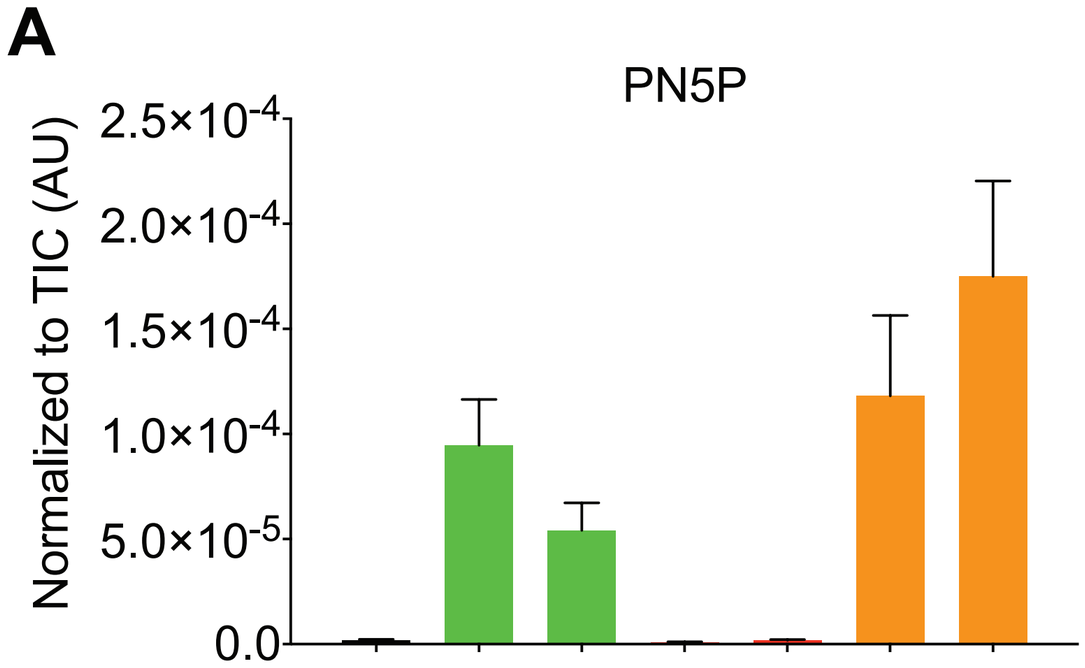
A
PN5P
Normalized to TIC (AU)
2.5×10-4
2.0×10-4
1.5×10-4
1.0×10-4
5.0×10-5
0.0

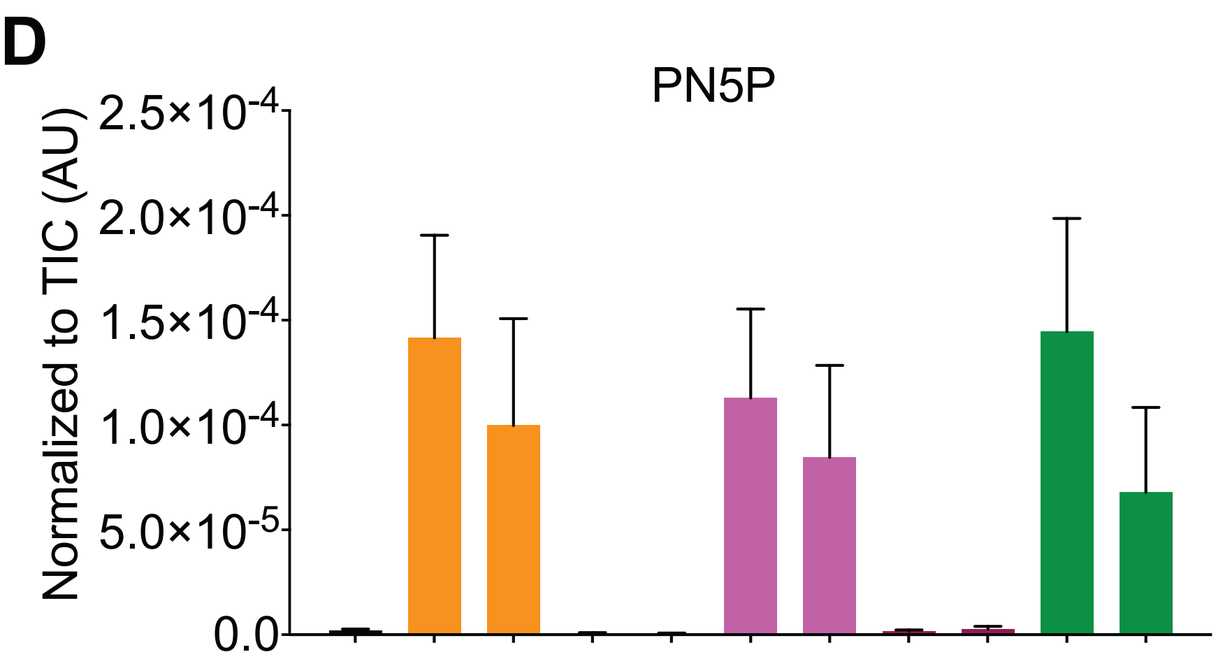
D
PN5P
Normalized to TIC (AU)
2.5×10-4
2.0×10-4
1.5×10-4
1.0×10-4
5.0×10-5
0.0

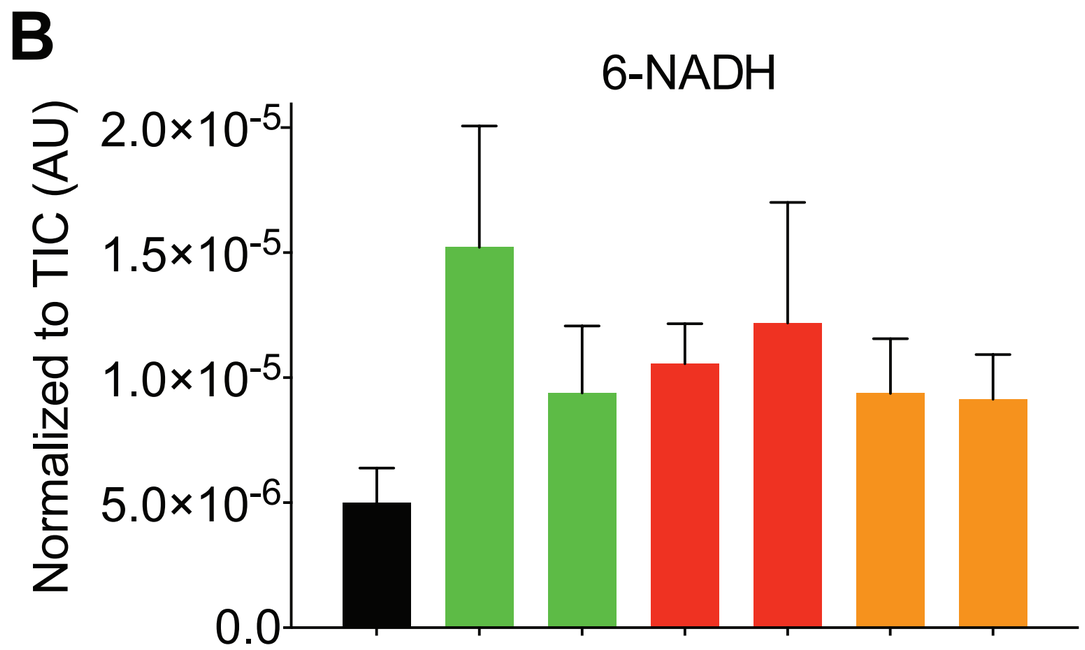
B
6-NADH
Normalized to TIC (AU)
2.0×10-5
1.5×10-5
1.0×10-5
5.0×10-6
0.0

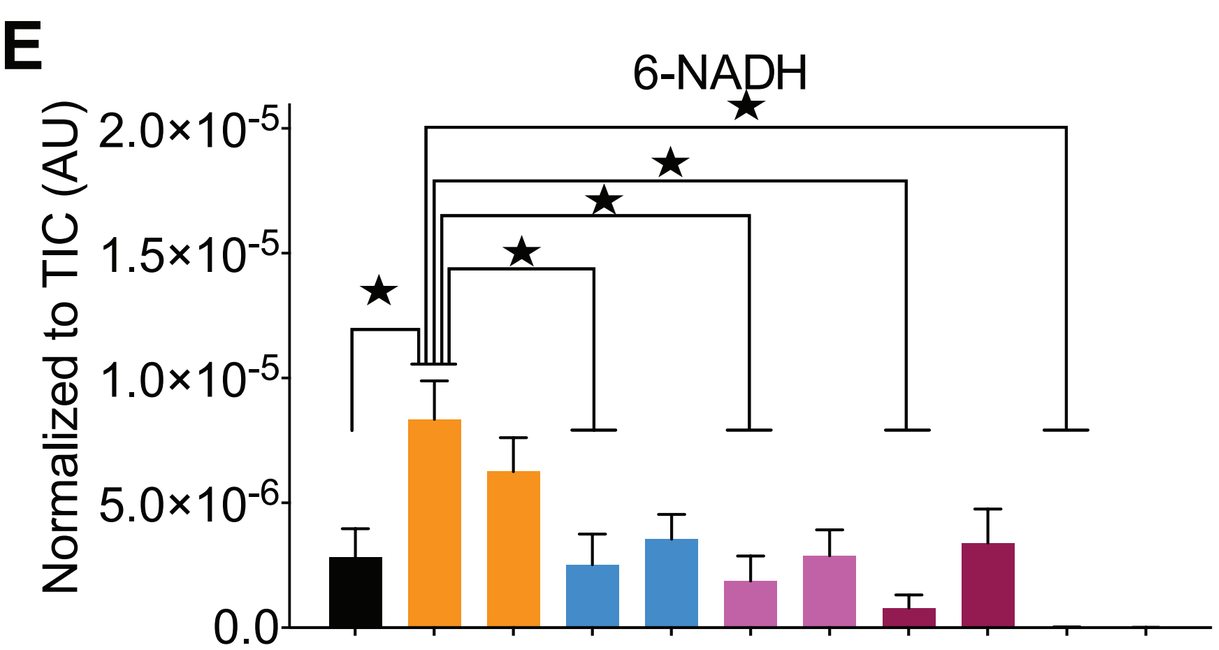
E
6-NADH
Normalized to TIC (AU)
2.0×10-5
1.5×10-5
1.0×10-5
5.0×10-6
0.0

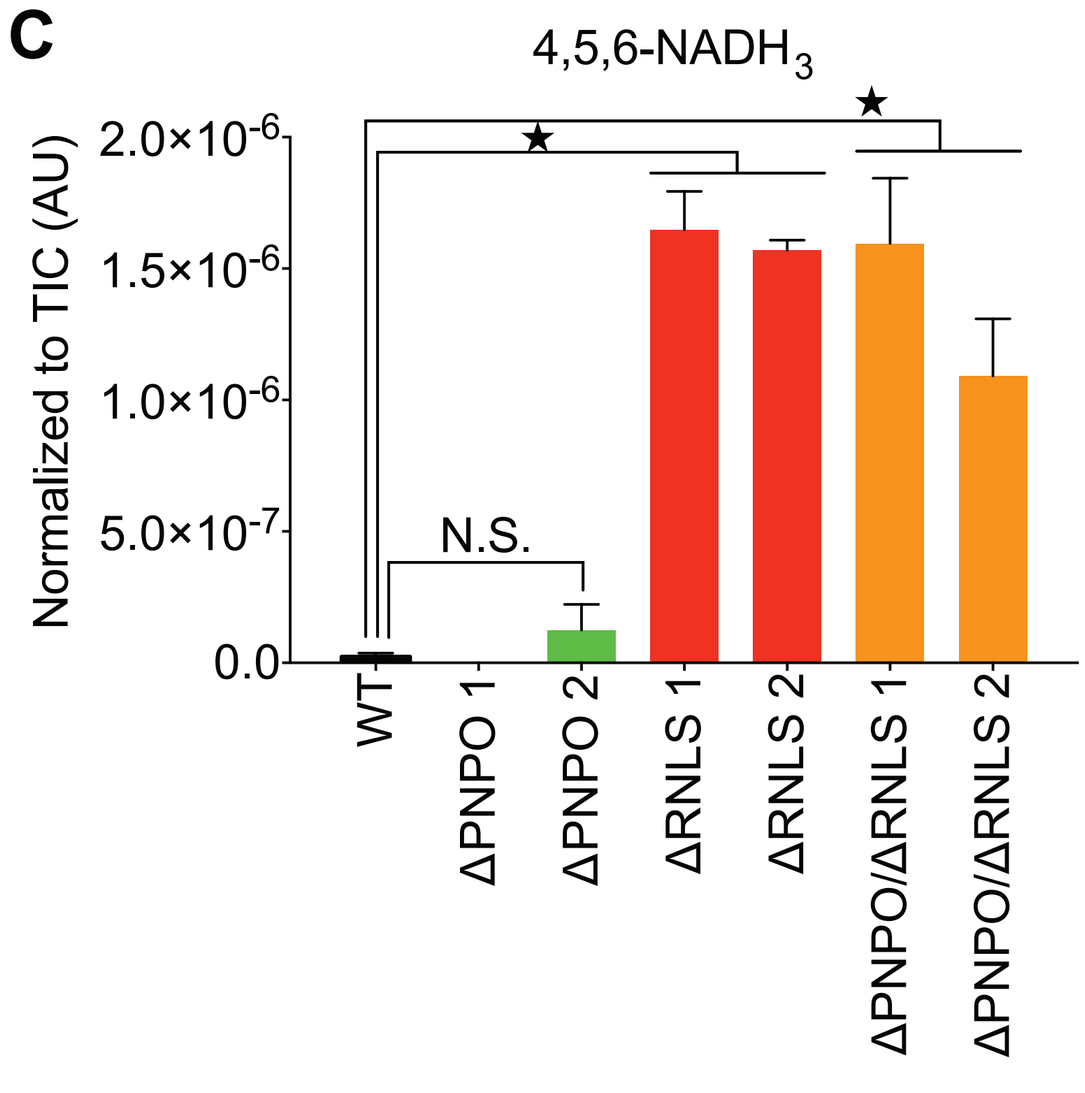
C
4,5,6-NADH3
Normalized to TIC (AU)
2.0×10-6
1.5×10-6
1.0×10-6
5.0×10-7
0.0
N.S.
WT
ΔPNPO 1
ΔPNPO 2
ΔRNLS 1
ΔRNLS 2
ΔPNPO/ΔRNLS 1
ΔPNPO/ΔRNLS 2

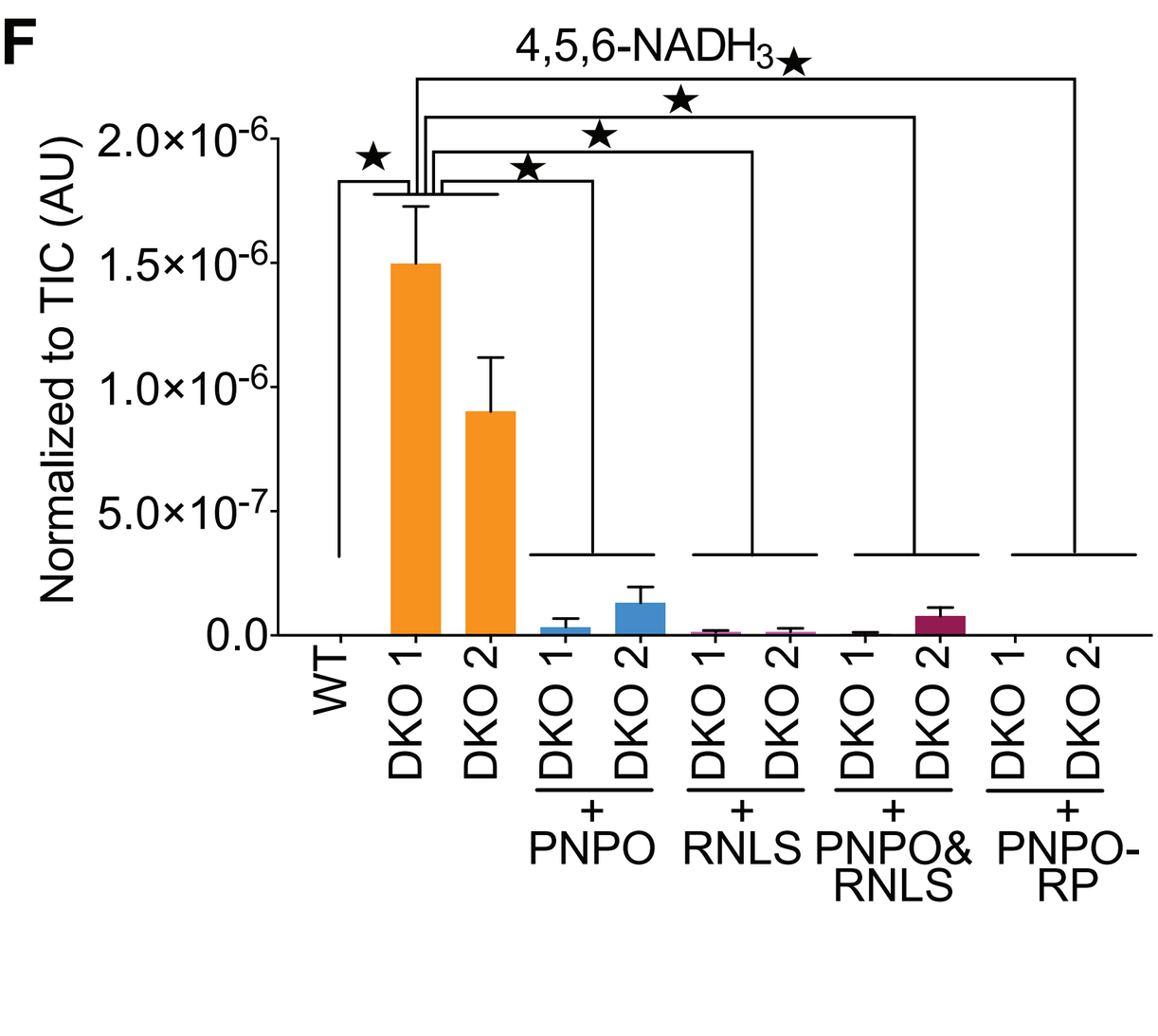
F
4,5,6-NADH3
Normalized to TIC (AU)
2.0×10-6
1.5×10-6
1.0×10-6
5.0×10-7
0.0
WT
DKO 1
DKO 2
DKO 1 + PNPO
DKO 2 + PNPO
DKO 1 + RNLS
DKO 2 + RNLS
DKO 1 + PNPO&RNLS
DKO 2 + PNPO&RNLS
DKO 1 + PNPO-RP
DKO 2 + PNPO-RP

Figure 8

A

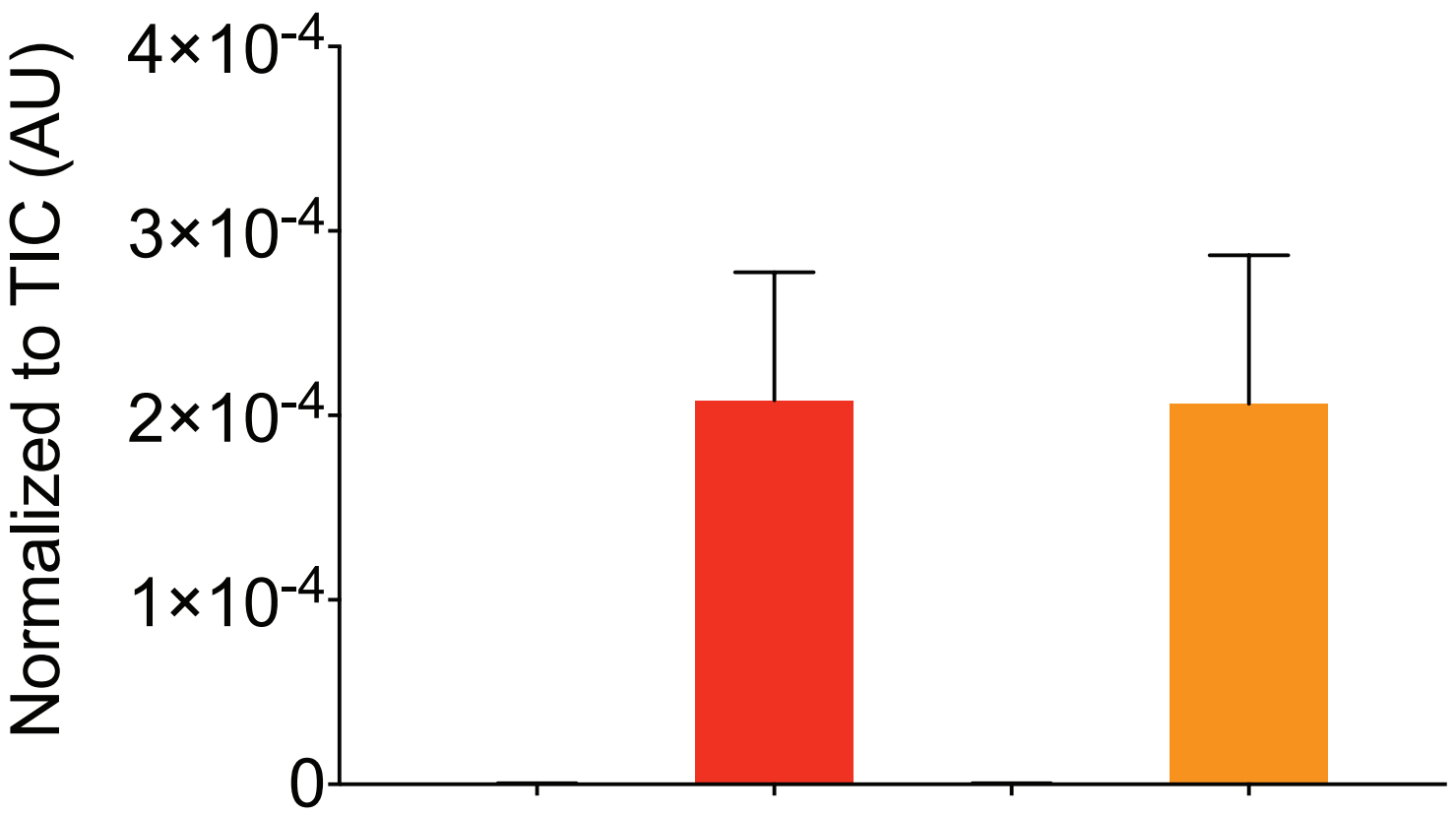
PN5P
Normalized to TIC (AU)
4×10-4
3×10-4
2×10-4
1×10-4
0

B

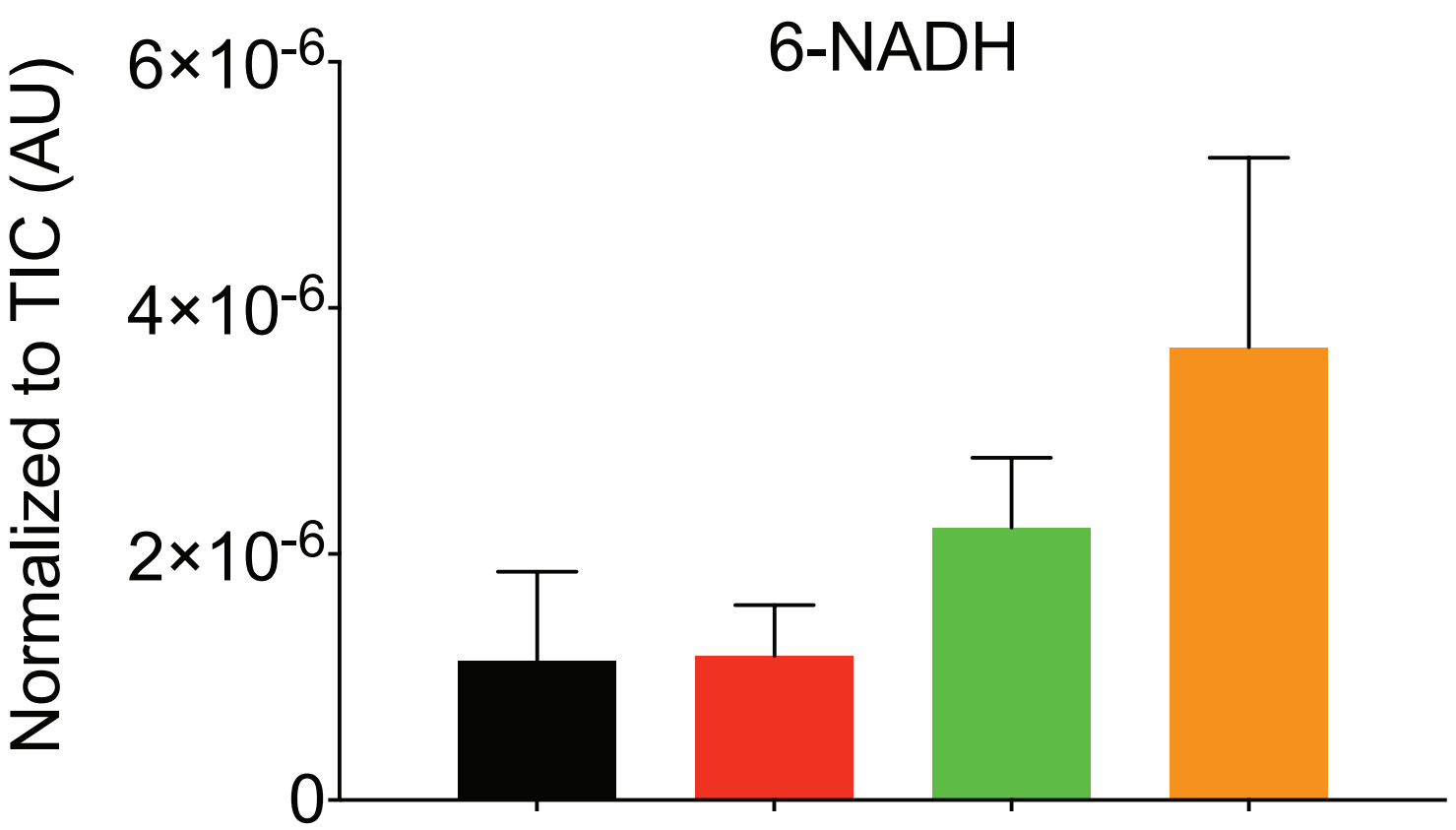
6-NADH
Normalized to TIC (AU)
6×10-6
4×10-6
2×10-6
0

C

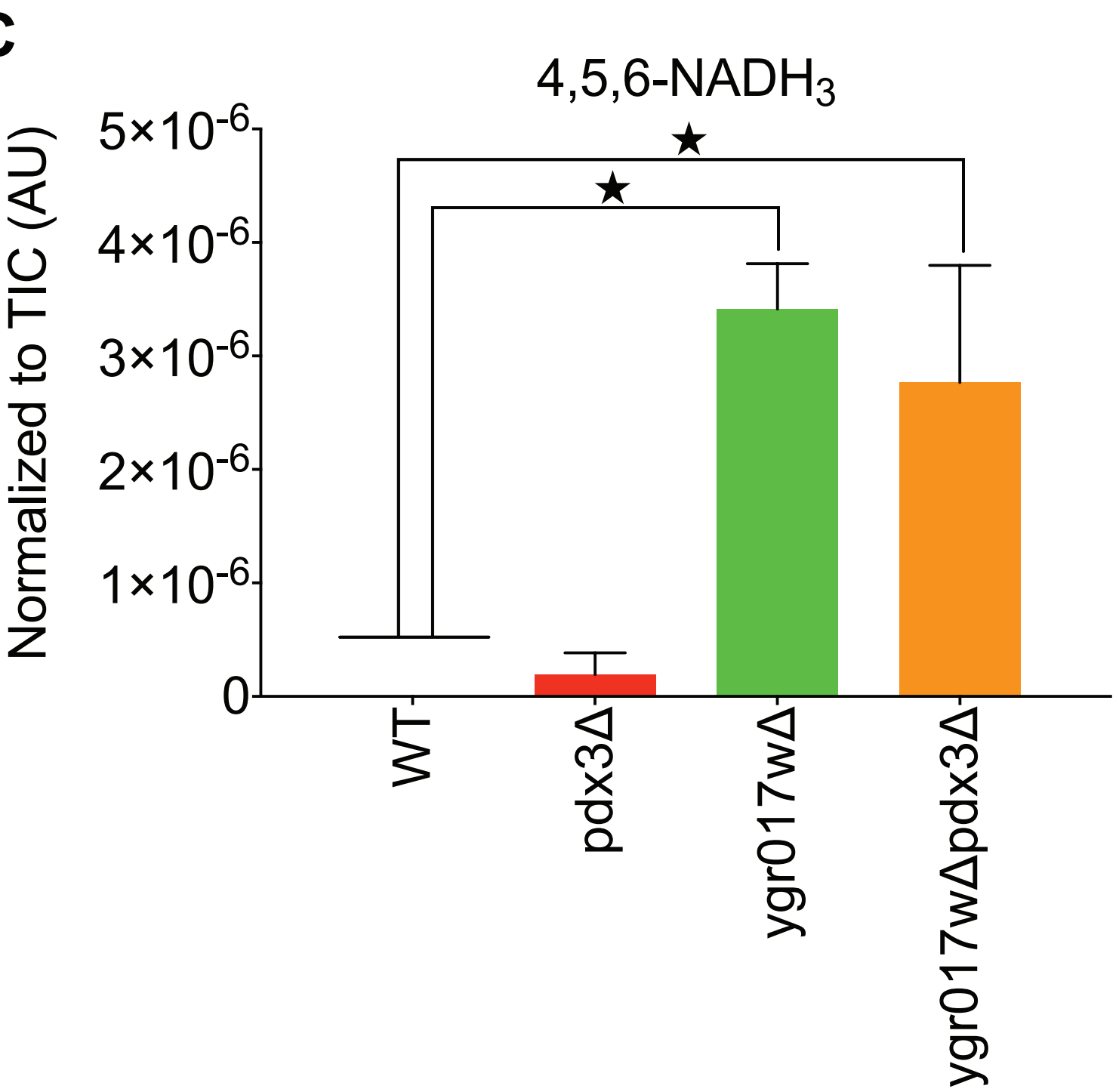
4,5,6-NADH3
Normalized to TIC (AU)
5×10-6
4×10-6
3×10-6
2×10-6
1×10-6
0
★
★
WT
pdx3Δ
ygr017wΔ
ygr017wΔpdx3Δ

Figure S1

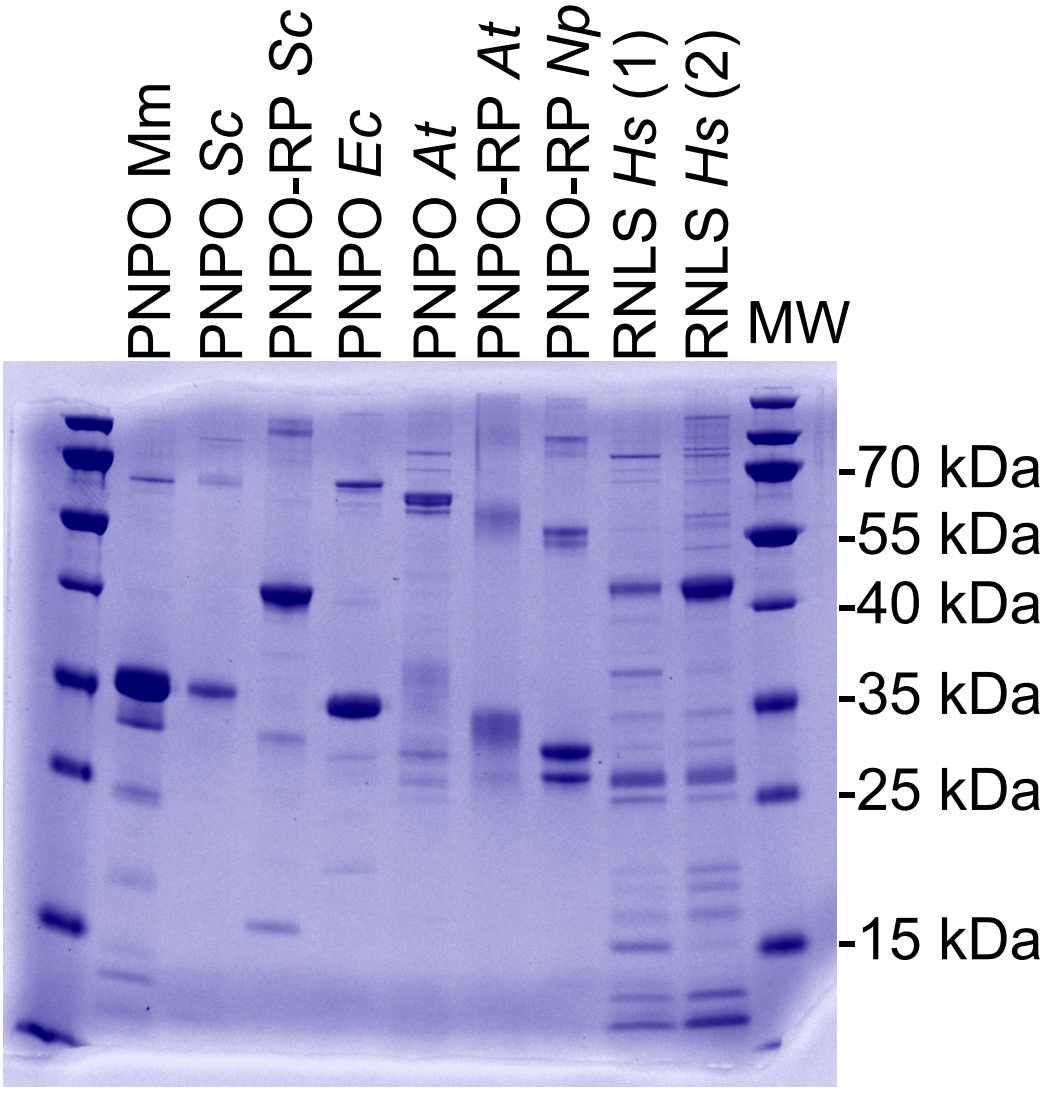
PNPO Mm
PNPO Sc
PNPO-RP Sc
PNPO Ec
PNPO At
PNPO-RP At
PNPO-RP Np
RNLS Hs (1)
RNLS Hs (2)
MW
-70 kDa
-55 kDa
-40 kDa
-35 kDa
-25 kDa
-15 kDa

Figure S2

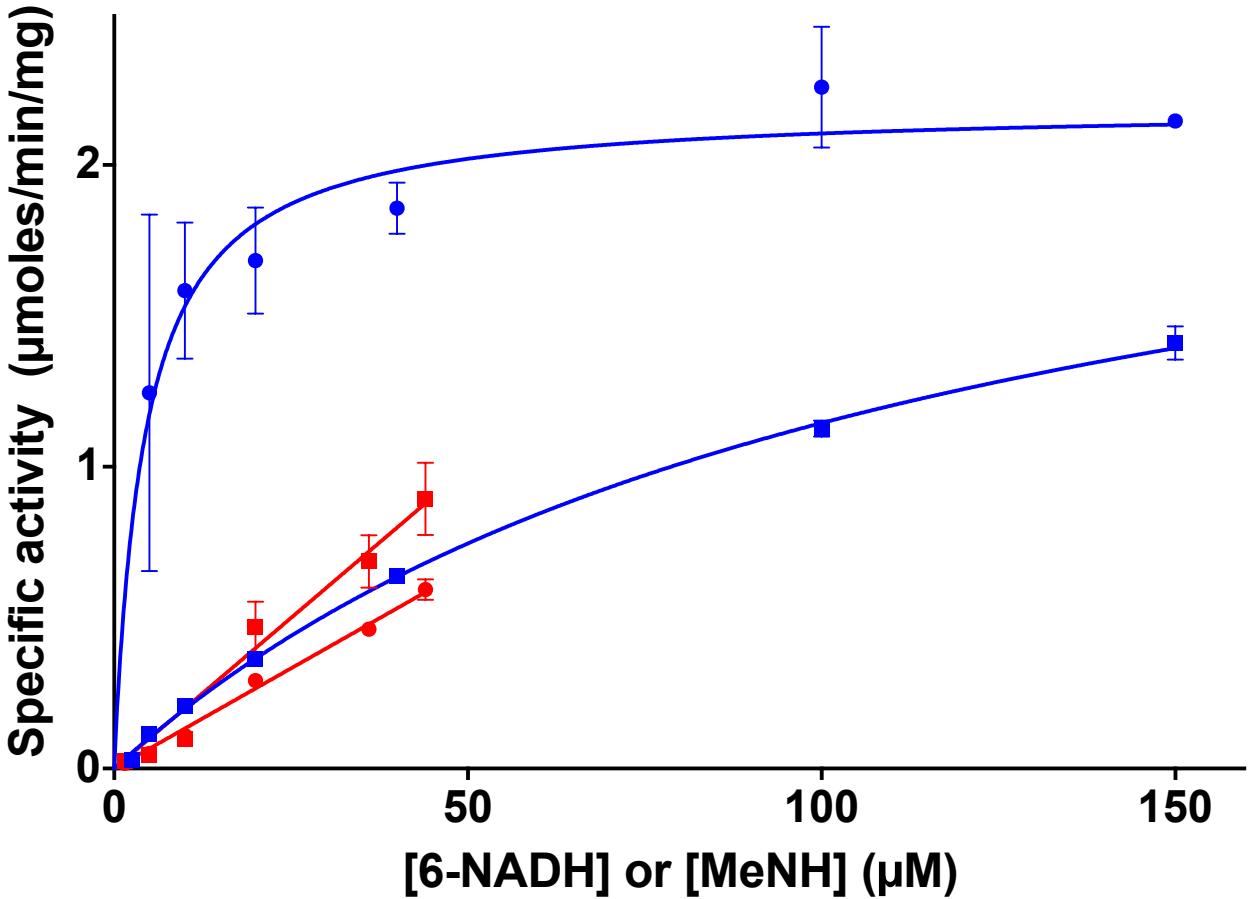
Specific activity (µmoles/min/mg)
0
1
2
0
50
100
150
[6-NADH] or [MeNH] (µM)

Figure S3

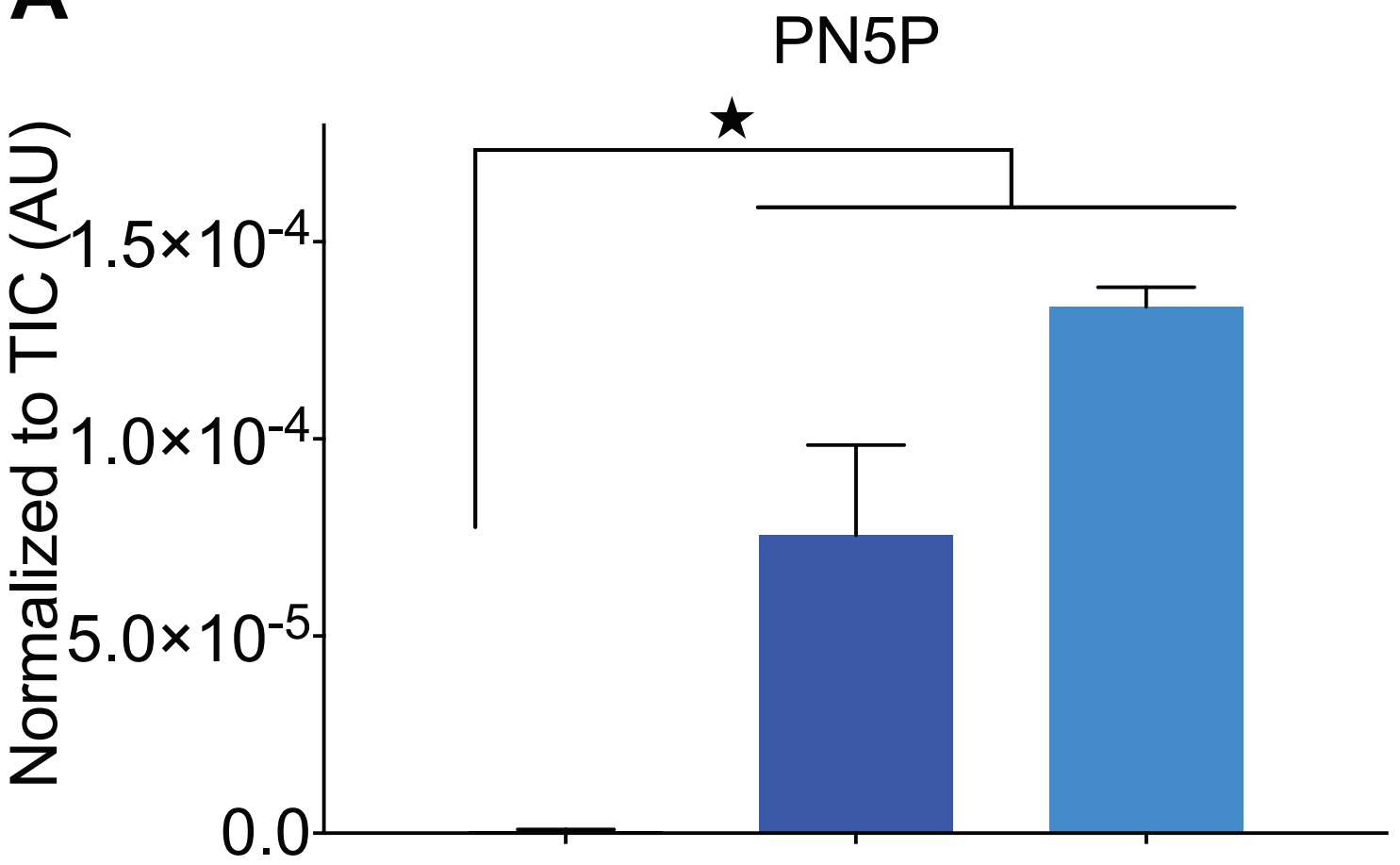
A
PN5P
Normalized to TIC (AU)
1.5×10-4
1.0×10-4
5.0×10-5
0.0

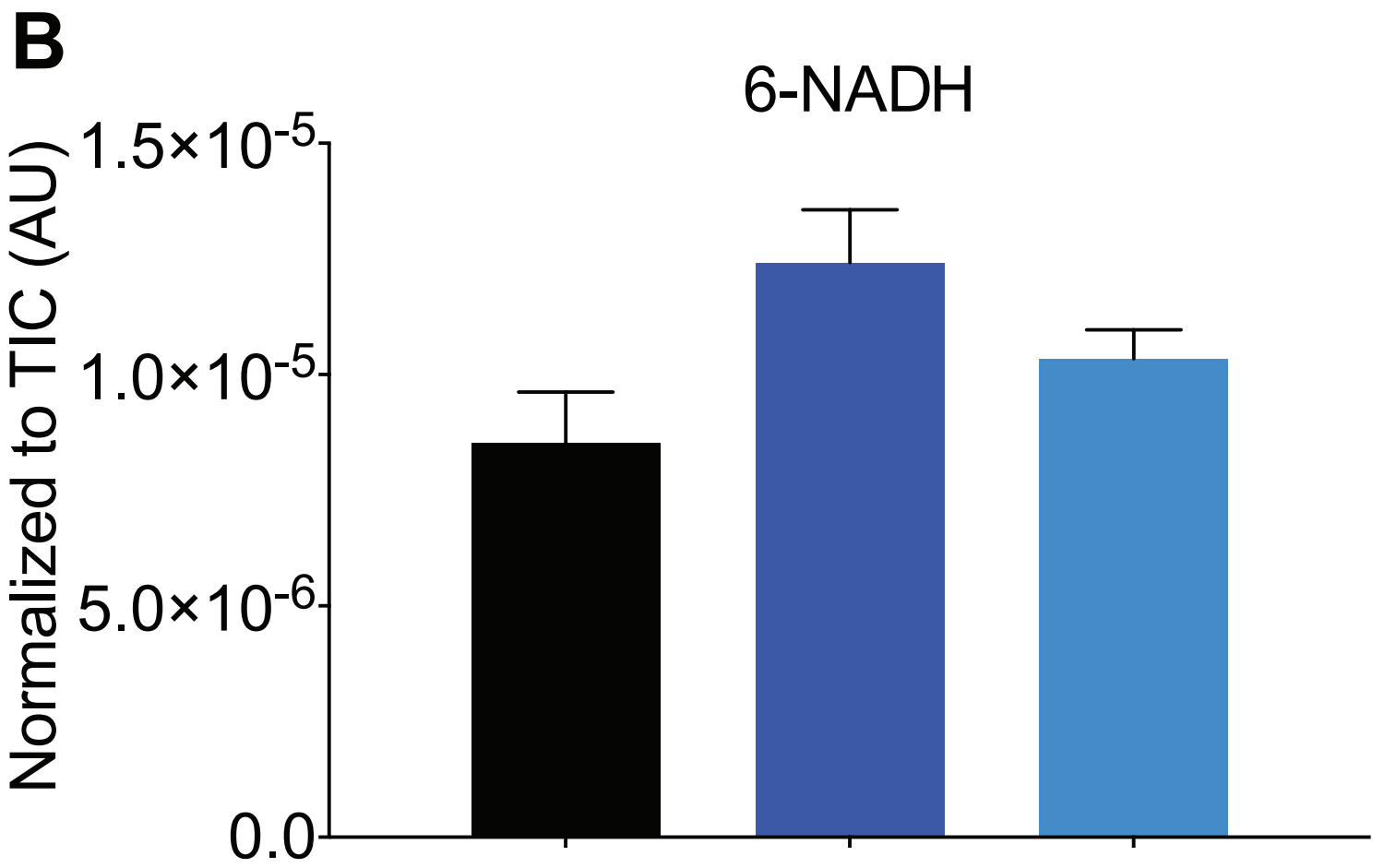
B
6-NADH
Normalized to TIC (AU)
1.5×10-5
1.0×10-5
5.0×10-6
0.0

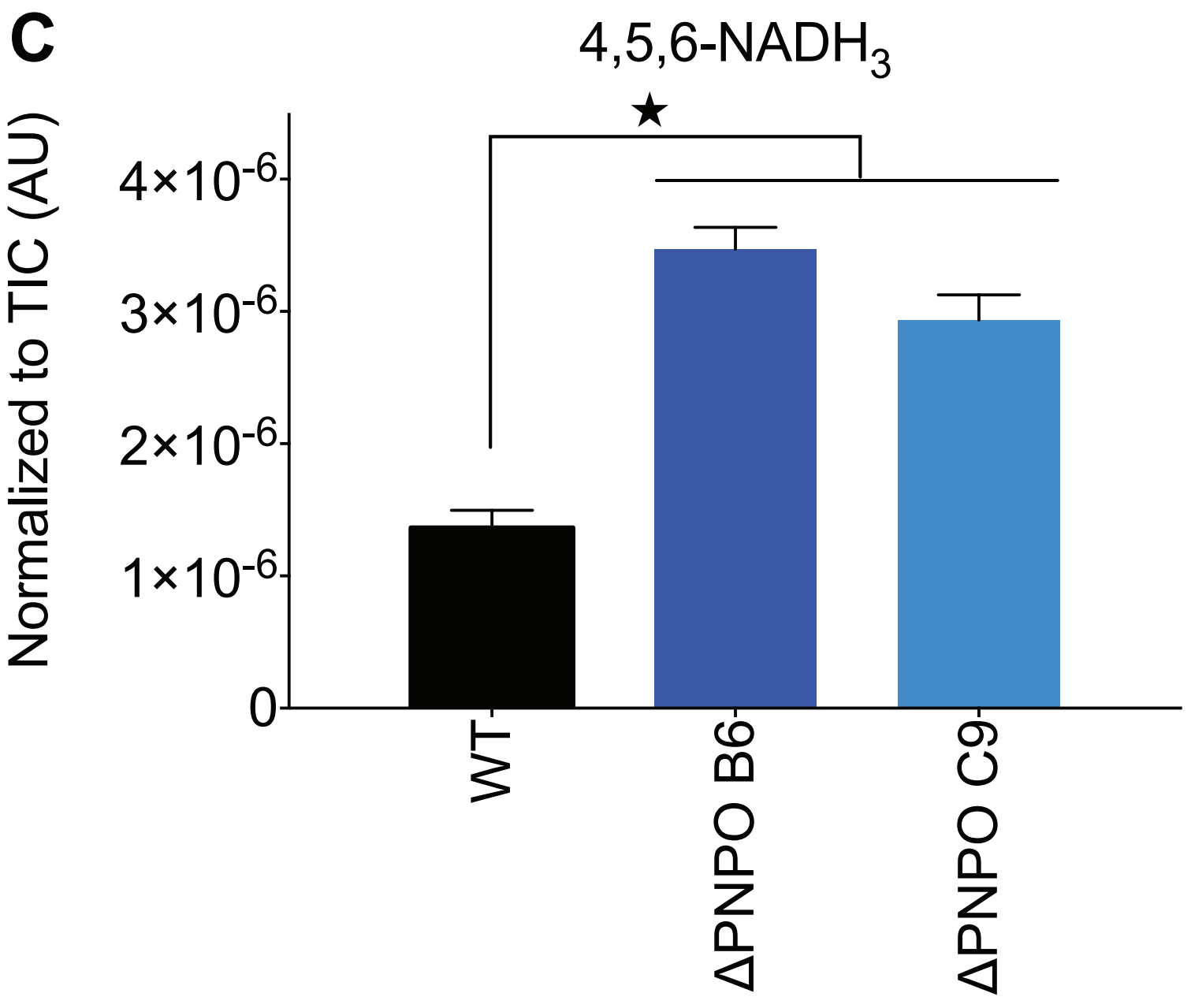
C
4,5,6-NADH3
Normalized to TIC (AU)
4×10-6
3×10-6
2×10-6
1×10-6
0
WT
ΔPNPO B6
ΔPNPO C9

SUPPLEMENTARY MATERIAL

Species	Gene	Source of DNA	DNA polymerase	5' primer	3' primer
Mus musculus	MmPNPO (PNPO)	Liver cDNA	Pfu	GCATGCTAGCATGGACCTGGGACCAATGC	TTTGCGGCCGCTTAAGGTGCAAGTCTCTCATAC
Saccharomyces cerevisiae	ScPNPO (Pdx3)	Genomic DNA	Pfu	CAGGAATTCCATATGATGACTAAACAAGCTGAGGAGACCC	CAGGAATTCGGTACCTCATGGGGCTAGTCTAACGACTTTCCATG
Escherichia coli	EcPNPO (PdxH)	ASKA clone	Pfu	CACCATGTCTGATAACGACGAATTGC	TCAGGGTGCAAGACGATC
Arabidopsis thaliana	AtPNPO (PPOX1)	Leaf cDNA	Phusion	CACCATGCAAGATTCAGGATCACC	TCATGGGGCCAATCTATG
Arabidopsis thaliana	AtPNPO-RP (PPOX2)	Leaf cDNA	Phusion	CACCATGGGAACACATGTAGCACC	TTATGGGTTAACCTTTTCTGAAGTC
Saccharomyces cerevisiae	ScPNPO-RP (Ygr017w)	Genomic DNA	Pfu	CACCATGTCGCATCAAATGGCGCC	TCACGGACACACTTCTTGTTC
Nostoc punctiforme	NpPNPO-RP (WP_012411992.1)	-	-	-	-
Homo sapiens	RNLS	Kidney cDNA	Phusion	CACCATGGCGCAGGTGCTGATC	CTAAATATAATTCTTTAAAGCTTCCAGAACACATAGG

Table S1 : Overview of the cloning of the genes of this study.
Mouse liver cDNA, yeast genomic DNA, ASKA clone collection (30), *A. thaliana* leaf cDNA (kind gift of M. Boutry, Catholic University of Louvain), or human kidney cDNA were used to amplify the genes of PNPOs, PNPO-RPs and RNLS. The proofreading DNA polymerase and the 5' and 3' primers used are listed.

Specie	Protein	Vector of expression	Restriction sites	Medium of expression	Temperature and duration of expression	Purification buffer
Mus musculus	MmPnpo (Pnpo)	pET28A	NheI and NotI	LB	37°C – 4h	50 mM Hepes pH 7.4
Saccharomyces cerevisiae	ScPnpo (Pdx3)	pET15b	NdeI and KpnI	LB	37°C – 4h	50 mM Hepes pH 7.4; 5 µM FMN
Escherichia coli	EcPnpo (PdxH)	pET100D-TOPO	-	LB	37°C – 4h	50 mM Hepes pH 7.4; 5 µM FMN
Arabidopsis thaliana	AtPnpo (PPOX1)	pET100D-TOPO	-	M9	30°C – 20h	50 mM Hepes pH 7.4; 5 µM FMN
A. thaliana	AtPnpo-RP (PPOX2)	pET100D-TOPO	-	M9	30°C – 20h	50 mM Hepes pH 7.4; 5 µM FMN
S. cerevisiae	ScPnpo-RP (Ygr017w)	pET100D-TOPO	-	M9	30°C – 20h	50 mM Hepes pH 7.4; 5 µM FMN
N. punctiforme	NpPnpo-RP	pSpeedET	-	M9 + AA	30°C – 20h	50 mM Hepes pH 7.4; 5 µM FMN
Homo sapiens	Rnls	pET100D-TOPO	-	M9 + AA	30°C – 20h	50 mM NaPi pH 8.0; 5 µM FAD; 10% glycerol

Table S2: Overview of the expression and the purification of the different recombinant proteins used in this study.

LB : Lysogeny Broth medium; M9 : Minimal Medium, containing 20 mM Glucose, 0.1 mM CaCl2, 2 mM $MgSO_4$; M9 + AA : Minimal Medium supplemented with 0.5 mg/l of biotin and thiamin and 0.1 g/l of casamino acid (Bacto).

Strain	Genotype	Name	Resistance	Source
BY4742	*Mat α*, ura3Δ0 ; leu2Δ0 ; his3Δ1 ; lys 2Δ0 0	WT	None	Euroscarf
Y13172	*Mat α*, ura3Δ0 ; leu2Δ0 ; his3Δ1 ; lys 2Δ0 ΔPdx3	*α* Ybr035c	Kanamycine	Euroscarf
Y14647	*Mat α*, ura3Δ0 ; leu2Δ0 ; his3Δ1 ; lys2Δ0 ΔYgr017w	*α* Ygr017w	Kanamycine	Euroscarf
Y04647	*Mat a*, ura3Δ0 ; leu2Δ0 ; his3Δ1 ; met15Δ0 ΔYgr017w	*a* Ygr017w	Kanamycine	Euroscarf
AM1	*Mat α Mat a*, ura3Δ0 ; leu2Δ0 ; his3Δ1 ; lys 2Δ0 ; met15Δ0 ΔPdx3ΔYgr017w	*α* ΔPdx3 *a* ΔYgr017w	Kanamycine	This study
AM2	*Mat a*, ura3Δ0 ; leu2Δ0 ; his3Δ1 ; lys 2Δ0 ΔPdx3ΔYgr017w	*a* ΔPdx3 ΔYgr017w	Kanamycine + hygromycine	This study
AM3	*Mat α*, ura3Δ0 ; leu2Δ0 ; his3Δ1 ; lys 2Δ0 ΔPdx3ΔYgr017w	*α* ΔPdx3 ΔYgr017w	Kanamycine + hygromycine	This study

Table S3: List of yeast strains used and designed for this study.

Primer	Sequence	Purpose
Pdx3KO_Fw	gatattttaaagatactctacctagaccagtagtacacttcacggatctgcactgTGCCATCTTTGTACAGCTTGCCT	Deletion of Pdx3 gene in the ΔYgr017w strain
Pdx3KO_Rv	gagagaattatatggtgttaaatagatcctacattgaatttttcattaacagtcccCGCAGAGCCGTGGCAGG	Deletion of Pdx3 gene in the ΔYgr017w strain
YgrKO_Fw	cgaggacctttcaccaaacaagaggaacttagctgatactaaacgaagattagTGCCATCTTTGTACAGCTTGCCT	Deletion of Ygr017w gene in the ΔPdx3 strain
YgrKO_Rv	gcgcgaatacaaagcattaaccatcgcgaacgttagcaataatgattgacatttcCGCAGAGCCGTGGCAGG	Deletion of Ygr017w gene in the ΔPdx3 strain
HpHB_Fw	ATGGGTAAAAAGCCTGAAC	Amplification of hygromycine resistance gene
HpHB_Rv	TTATTCCTTTGCCCTCGG	Amplification of hygromycine resistance gene
Pdx3_upS_Fw	GAGCTCTTATAGATGCCACCAG	Amplification with HpHB primers to verify that the resistance cassette is inserted in the good place in the genome
Pdx3_downS_Rv	CGCCATTTCCAAATTTCG	
Ygr_upS_Fw	GAGAGTAAGTCGAGCACG	
Ygr_downS_Rv	GGTAAAATCGCCGACG	

Table S4: List of primers used to design the *pdx3*Δ*ygr017w*Δ yeast cells and verify the correct gene disruption. Capital letters in the first four primers correspond to nucleotides homologous to the flanking regions of the hygromycine cassette.

Primer	Sequence
CRISP-PNPOe3-s1	CACCGGACTAACTTCGAGAGTCGAAA
CRISP-PNPOe3-as1	AAACTTTCGACTCTCGAAGTTAGTCC
CRISP-PNPOe3-s2	CACCGGCAGCAGCAACATGCGAGCAG
CRISP-PNPOe3-as2	AAACCTGCTCGCATGTTGCTGCTGCC
CRISP-PNPOe5-s3	CACCGGTTCTGTGATCCCTGATCGGG
CRISP-PNPOe5-as3	AAACCCCGATCAGGGATCACAGAACC
CRISP-RNLSe2-s1	CACCGGCCTTGCAACTAACTCACCGT
CRISP-RNLSe2-as1	AAACACGGTGAGTTAGTTGCAAGGCC
CRISP-RNLSe2-s2	CACCGGCTGTGCACTGAGGATTATG
CRISP-RNLSe2-as2	AAACCATAATCCTCAGTGCACAGCC
CRISP-RNLSe5-s3	CACCGGAGGCCCAGAGCATATCGAG
CRISP-RNLSe5-as3	AAACCTCGATATGCTCTGGGCCTCC
CRISP-RNLSe5-s4	CACCGGTTGGCATTCACTAATTACTG
CRISP-RNLSe5-as4	AAACCAGTAATTAGTGAATGCCAACC

Table S5: List of primers used to design the CRISPR/Cas9 HCT116 ΔPNPO, U2OS ΔPNPO, U2OS ΔRNLS and U2OS ΔPNPOΔRNLS cell lines.

Primer	Sequence
pLVX_PNPOs	atacat**GGATCC**CCACCATGACGTGCTGGCTGC
pLVX_PNPOas	atgtat**TGTACA**TTAAGGTGCAAGTCTCTCATAGAG
pLVX_RNLSs	atacat**GGATCC**CCACCATGGCGCAGGTGCTGATC
pLVX_RNLSas	atgtat**TGTACA**CTAAATATAATTCTTTAAAGCTTC
pLVX_PPOX2s	atacat**GGATCC**CCACCATGGGAACACATGTAGCAC
pLVX_PPOX2as	atgtat**TGTACA**TTATGGGTTAACCTTTTCTGAAG

Table S6: List of primers used to complement ΔPNPO, ΔRNLS and ΔPNPO/ΔRNLS U2OS cell lines via the generation of a retroviral expression vector. Bold types indicate restriction sites.

Primer	Sequence
Mm_Pnpo_p2s	TCGAGAGGCATTCGAGGAGA
Mm_Pnpo_p2as	TGAACAGCCTCGTCAAACCA
Mm_Rnls_p3s	GAGGAACTGTTAGCTCATGGAA
Mm_Rnls_p3as	GGAGACTTCTGCACCTGACTTT
Mm_TBP_p1s	ACCTTATGCTCAGGGCTTGG
Mm_TBP_p1as	GCCATAAGGCATCATTGGAC

Table S7: List of primers used for the qPCR experiments on cDNA of mice tissues.

Accession	Description	Blue Trisacryl		Phenyl Sepharose		Enrichment Ratio
		PSM Number	PSM Normalized	PSM Number	PSM Normalized	
IPI00191737.6	Serum Albumin	215	41.75	318	42.91	1.03
IPI00231745.8	Fructose-1,6-Bisphosphatase 1	59	11.46	26	3.51	0.31
IPI00205157.1	Hydroxyacyl-CoenzymeA Dehydrogenase	20	3.88	0	0	0
IPI00207601.1	Hydroxyacid Oxidase 1	18	3.50	29	3.91	1.12
IPI00210823.1	3-oxo-5-Beta-steroid 4-Dehydrogenase	16	3.11	25	3.37	1.08
IPI00212603.1	Pyridoxine-5'-phosphate Oxidase	13	2.52	51	6.88	2.73
IPI00193258.7	Phenylalanine-4-hydroxylase	11	2.14	11	1.48	0.69
IPI00197696.2	Malate Dehydrogenase, mitochondrial	11	2.14	9	1.21	0.57
IPI00212015.1	Medium-Chain Specific Acyl-CoA Dehydrogenase	11	2.14	2	0.27	0.13
IPI00324633.2	Glutamate Dehydrogenase 1, mitochondrial	11	2.14	0	0	0
IPI00454559.2	Txnrd 1 protein	11	2.14	15	2.02	0.94
IPI00211507.3	4-hydroxyphenylpyruvate dioxygenase	10	1.94	8	1.08	0.56
IPI00193485.2	Isocitrate Dehydrogenase [NADP], mitochondrial	6	1.17	4	0.54	0.46
IPI00339188.2	3-hydroxyanthranilate 3,4-dioxygenase	5	0.97	14	1.89	1.95

Table S8: Table showing the enrichment ratio of the 12 oxidoreductases identified in the peak activity fractions after Blue-Sepharose and Phenyl-Sepharose purification steps. Proteins present in the peak fractions of 6-NADPH-oxidase activity in the Blue-Sepharose and Phenyl-Sepharose chromatography were digested with trypsin and analysed by LC-MS-MS. Among the 12 oxidoreductases identified, two were enriched at least two-fold after the Phenyl-Sepharose step (highlighted in yellow) : 3-hydroxyanthranilate 3,4-dioxygenase and pyridox(am)ine-5'-phosphate oxidase (PNPO).

LEGEND TO SUPPLEMENTARY FIGURE

Figure S1: SDS-PAGE analysis of the purified recombinant proteins. The following purified recombinant protein were submitted to SDS-PAGE analysis and Coomassie Blue staining : Mus musculus PNPO (theoretical mass of the subunit with the polyHis-tag : 30.6 kDa); Saccharomyces cerevisiae PNPO (Pdx3; 30.9 kDa); Saccharomyces cerevisiae PNPO-RP (Ygr017w; 42.8 kDa) ; Escherichia coli PNPO (PdxH; 29.5 kDa); Arabidopsis thaliana PNPO (PPOX1; 63.4 kDa); Arabidopsis thaliana PNPO-RP (AtPPOX2; 30.7 kDa); Nostoc punctiforme PNPO-RP (NpPPOX2; 26.5 kDa); Homo sapiens renalase (two preparations; 41.8 kDa).

Figure S2: Effect of mutation of Arg45 residue on the enzymatic efficiency of *N. punctiforme* PNPO-RP. Enzymatic activity of wild-type (circles) or of R45A mutant (squares) of *N. punctiforme* recombinant PNPO-RP was assayed on 6-NADH (blue lines) or on reduced N-methylnicotinamide (MeNH – red lines) at 345 nm as described in Experimental. The concentration of enzyme used in the assays were ≈ 0.1 µM for the assays of the wild-type protein with 6-NADH and ≈ 0.6 µM for all other assays. The extinction coeficient of both 6-NADH and 6-MeNH at 345 nm used to determine the activities was 6580 $M^{-1}.cm^{-1}$. Results shown are means ± SD for 3 determinations. K_M and V_{max} were calculated with the Prism software.

Figure S3: Effect of inactivation of the PNPO gene on the amount of pyridoxine-5'-P, 6-NADH and 4,5,6-$NADH_3$ in HCT116 cells.
Wild type (WT) cells and two single mutant clones (ΔPNPO B6 or C9) were analysed by LC/MS. Pyridoxine-5'-P (A), 6-NADH (B) and 4,5,6-$NADH_3$ (C) were quantified. The peaks obtained by LC-MS were divided by the Total Ion Current (TIC) of the chromatogram. Means ± SEM for $n \geq 3$. Statistical analyses were performed by student t-test.